January 2016

Quantifying Cure In Industrial Composites Using Fourier Transform Infrared Spectroscopy (FTIR)

Jason Robert Burns

Follow this and additional works at: https://commons.und.edu/theses

QUANTIFYING CURE IN INDUSTRIAL COMPOSITES USING FOURIER
TRANSFORM INFRARED SPECTROSCOPY (FTIR)

by

Jason R. Burns
Bachelor of Science, University of North Dakota, 2015
Master of Science, University of North Dakota, 2016

A Thesis

Submitted to the Graduate Faculty

of the

University of North Dakota

in partial fulfillment of the requirements

for the degree of

Master of Science

Grand Forks, North Dakota
December
2016

This thesis, submitted by Jason R. Burns in partial fulfillment of the requirements for the Degree of Master of Science from the University of North Dakota, has been read by the Faculty Advisory Committee under whom the work has been done and is hereby approved.

_____
Chairperson (Dr. Matthew Cavalli)

_____
Dr. Surojit Gupta

_____   12/8/2016
Dr. William Semke

This thesis is being submitted by the appointed advisory committee as having met all of the requirements of the School of Graduate Studies at the University of North Dakota and is hereby approved.

_____
Dr. Grant McGimpsey
Dean of the School of Graduate Studies

December 8, 2016
_____
Date

PERMISSION

Title Quantifying Cure in Industrial Composites Using Fourier
 Transform Infrared Spectroscopy (FTIR)

Department Mechanical Engineering

Degree Master of Science

  In presenting this thesis in partial fulfillment of the requirements for a graduate
degree from the University of North Dakota, I agree that the library of this University
shall make it freely available for inspection. I further agree that permission for extensive
copying for scholarly purposes may be granted by the professor who supervised my
thesis work or, in his absence, by the Chairperson of the department or the dean of the
School of Graduate Studies. It is understood that any copying or publication or other use
of this thesis or part thereof for financial gain shall not be allowed without my written
permission. It is also understood that due recognition shall be given to me and to the
University of North Dakota in any scholarly use which may be made of any material in
my thesis.

<div align="right">

Jason R. Burns

December 2016

</div>

TABLE OF CONTENTS

LIST OF FIGURES

LIST OF TABLES

ACKNOWLEDGMENTS

ABSTRACT

A study has been taken to evaluate the utility of two Fourier transform infrared (FTIR) spectroscopic sampling methods in calculating the degree of cure in an industrial fiberglass-reinforced composite material. Methodologies examined include: attenuated total reflectance (ATR) and diffuse reflectance (DRIFTs), both which utilize the Agilent 4100 ExoScan FTIR platform. As the formulation of the unsaturated polyester resin used in the fabrication of the industrial composite is proprietary a cure model based on the plasticizer, styrene, is proposed. Results of the infrared tests show that neither the resolution of ATR FTIR or DRIFTs is sufficient to monitor cure of the polyester resin in real time. With a 95% confidence interval, cure states between 24 and 120 hours after resin infusion cannot be differentiated. Statistical significance can be noted, however; between pre- and post-processed samples which have been cured for an addition 14 hours at 60ºC. The methodology for calculating degree of cure, subsequent results and statistical analysis are presented.

CHAPTER ONE: INTRODUCTION

In the world of structural materials there are four basic categories: metals, polymers, ceramics, and composites. A composite material is one brought about by mixing materials differing in composition or form on the macroscopic level for the purpose of obtaining enhanced properties and/or physical characteristics [1]. For most structural applications, the components of a composite can be broken into two categories: the matrix and the reinforcing particulate or fiber. One class of structural composites commonly used in manufacturing today are classified as laminar fiber composites, comprising many stacked layers of fibers (typically glass- or carbon-based) bonded together by a polymer matrix.

Polymers can be classified into one of three groups with respect to degree of reticulation, or extent of cross-linking: thermoplastics, elastomers, and thermosets. Cross-links are chemical bonds which link one polymer chain to another, adding rigidity to the structure. Thermoplastic polymers have little or no interchain cross-linking. This means they are often solvent-soluble and flow easily. Elastomers have a slight degree of cross-linking which prevents chains from sliding past one another when stretched, giving these materials their elasticity. The third classification of polymers are thermosets which are heavily cross-linked to the point of irreversibility [2].

Unsaturated polyester (UP) is the thermoset of choice in a variety of industrial composite manufacturing applications. Examples include: wind turbine blades, sports equipment, and aerospace, automotive, and marine components. A UP resin consists of an acid or anhydride and

an alcohol or polyol as well as various other additives. While some additives are used to alter physical properties such as color and scent, additives such as styrene and the introduction of an initiator are crucial in determining the cure kinetics of the UP resin [2]. The initiator, typically a peroxide, is added to the UP resin along with styrene. Upon decomposing, the initiator gives off free radicals which then react with both the polyester and styrene forming long, interconnected polymer chains. It is the concentration of these complex cross-linked chains which determines the degree of cure (DOC) of the material [2,3].

In industry, quantifying the degree of cure is an important step in insuring a product has been manufactured properly. Traditionally, monitoring the cure process has been done using destructive testing processes such as differential scanning calorimetry [2,3], or by way of mechanical testing [2]. Although effective, these processes are labor-intensive and time-consuming; it is for these reasons a non-destructive testing technique is desirable.

As the curing process of the UP resin is a series of chemical reactions, a possible way to monitor the cure process is using an instrument long used in the field of analytical chemistry. Fourier transform infrared (FTIR) spectroscopy looks at the interaction of infrared light with matter; this light vibrates individual atoms which absorb a fraction of the emitted energy. The energy at which a peak in the spectrum appears corresponds to the frequency of vibration of an individual chemical bond of the sample molecule [4-6]. FTIR has become increasingly popular as advances in technology reduce the size of a once large, bulky desktop FTIR unit to one that can be carried around in the palm of your hand. The degree of cure in a UP resin sample can be calculated by monitoring the normalized absorbances at the reaction sites over the span of the entire cure cycle. This data is compiled to create a calibration curve which is then stored in the

FTIR unit to instantaneously determine the degree of cure of any production part made of the same material [3].

The work presented will examine two popular FTIR methods and evaluate their utility in calculating DOC in a laminar fiber composite material. The composite used in the study consists of HM-glass fibers bound in an unsaturated polyester resin matrix. The resin was first analyzed using a Thermo Scientific Nicolet iS5 in transmission mode to learn more about the cure history and ensure the accuracy of our DOC model. Large plates of composite material were then manufactured using a vacuum assisted resin transfer molding (VARTM) process. Batches of samples were cut from the plate of material in post-processed in a variety of ways. Attenuated total reflectance (ATR) FTIR (Agilent 4100 ExoScan) was then used to monitor the relative change in cure as a result of post-processing. In addition to ATR, a diffuse reflectance attachment for the Agilent 4100 ExoScan FTIR unit was also evaluated for utility.

This work is of importance due to its practical applications in industry. A global wind turbine blade producer is interested in monitoring cure to use as a process control benchmark. In order for this manufacturer to ship a blade to a customer, they first must be certain the curing reaction has been completed. Currently, a digital thermometer is embedded in each blade produced at their factory. As the curing of the polyester resin matrix is an exothermal process, the thermometer can monitor the heat of the reaction if other variables are held consistent. The cure of a blade is deemed complete if the thermometer records a particular temperature for a specified duration. This method requires extra processing of the data collected by the temperature stick and may be an indirect measure of degree of cure if, for example, the blades are moved into colder air. A direct measurement of degree of cure is desired. Employing FTIR would also allow the same cure analysis to be completed in the matter of minutes in real-time

without the need to embed a sensor and process the data after manufacturing has already been completed.

Following this introduction, Chapter 2 will provide a general overview of FTIR theory, a discussion of various sampling techniques and offer an overview of relevant research previously conducted in this field. Next, Chapter 3 will discuss the materials and experimental methods used throughout this study. Finally, Chapter 4 will provide a comprehensive summary of the results before concluding with recommendations for further study in Chapter 5.

CHAPTER TWO: BACKGROUND

Calculating the degree of cure (DOC) of a polymer requires careful consideration of the chemical reactions taking place and can be done by monitoring any number of intrinsic parameters. Traditionally, DOC has been calculated in one of three ways: calorimetry, dynamic mechanical analysis, or rheometry [2]. Polymeric chemical reactions most often result in the release or absorption of heat. Using a calorimeter, it is possible to monitor the cure process of a thermosetting system. For most thermosetting polymers, the cross-linking reaction is temperature-dependent and can accurately be described using a simple Arrhenius relationship as outlined in Eq. 1

$$\ln k = \ln A - \frac{E_a}{RT} \tag{1}$$

where k is the reaction rate, A is the pre-exponential factor, E_a is the activation energy of the system, R is the universal gas constant, and T is the absolute temperature [2].

Dynamic mechanical analysis monitors the change in Young's modulus of a thermoset as it cures, and similarly, rheometry relates the change in viscosity to the DOC of a polymer [2]. These three methods are simple and effective but share two crucial drawbacks: none are universal and all require a sacrificial sample. Fourier transform infrared spectroscopy (FTIR) aims to calculate the DOC without needing to rely on intrinsic parameters, instead focusing on the alteration of chemical bonds, an attribute common to all polymerization reactions regardless of composition.

2.1 FTIR Basics

Infrared spectrometry equipment has been a staple of analytical laboratories across the country since it became commercially available in the mid 1940's [4]. Until very recently the primary use of such an instrument has been to provide information about molecular structure which can be determined by studying the patterns of characteristic absorbance bands present in the infrared (IR) spectrum. While this was an effective tool for determining the presence of particular functional groups in a molecule, the first infrared spectrometers were large and often quickly replaced by multi-functional instruments such as a mass spectrometer or an x-ray diffraction device. Because of this the technology went largely neglected until the implementation of the Fast Fourier Transform algorithm. This is a mathematical implementation which transforms the raw data collected by FTIR into an interpretable spectrum through a series of steps to account for instrumental imperfections and basic scanning limitations. Combining this breakthrough with the increasing miniaturization of electronic components and by the late 1990's FTIR had become an attractive option for many different analytical applications [4-7]. Currently, scientific instrument manufacturers such as Agilent [8], and Thermo Scientific [9] market handheld FTIR devices designed for field use.

2.1.1 FTIR Components

All FTIR spectrometers contain an IR source, interferometer, and an IR energy detector. In its simplest form, the interferometer consists of a beamsplitter, a fixed mirror, and a constant-velocity mirror. IR radiation from the source is split into two different components by the beamsplitter. These two IR beams are then re-combined and pass through the sample. Any radiation which has not been absorbed is then delivered to the detector. The constant-velocity mirror creates a pattern of constructive and destructive interference of all the wavelengths of IR

radiation simultaneously; this pattern is called the interferogram. Absorbed wavelengths of radiation do not appear on the interferogram. Since each molecule absorbs varying wavelengths, each interferogram is molecule-specific, analogous to a human fingerprint. In order to improve readability, the interferogram is converted from the time-distance domain to the frequency domain using the Fast Fourier Transform algorithm, resulting in the characteristic IR spectrum of that sample [4-7]. Figure 1 shows an example of an IR spectrum, the intensity of absorption is plotted against the radiation wavenumber, or inverse of wavelength.
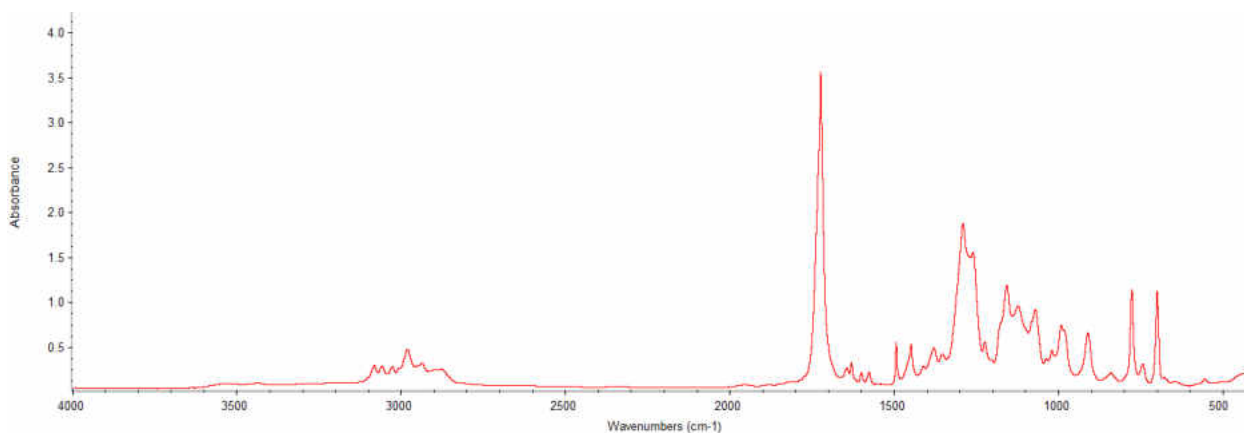
Figure 1: IR spectrum of Polylite 413-575 unsaturated polyester resin (GT-125)

2.1.2 Atomic Vibrations and the IR Spectrum

An IR spectrum is a plot of relative IR absorbance (or transmittance) of a material at a given vibrational frequency. IR radiation is absorbed by a material by converting the energy into atomic vibrations. The energy absorbed by an atomic bond can lead to a change in bond length (stretching) or bond angle (bending). These two normal modes vibrate at a given frequency based on the bond stiffness and the reduced mass of the bonded atoms or functional groups [4].

For a simple two atom system, the reduced mass can be calculated as shown in Eq. 2, and the resultant frequency of absorption can be calculated as shown in Eq. 3

$$\frac{1}{\mu} = \frac{1}{m_1} + \frac{1}{m_2} \tag{2}$$

$$v = \frac{1}{2\pi}\sqrt{\frac{k}{\mu}} \tag{3}$$

where μ is the reduced mass derived from the individual masses of the two atoms, m_1 and m_2, v is

the frequency of absorption and k the force constant, a measure of the bond stiffness. The

intensity of the infrared band on the spectrum is a function of the change in the dipole moment of

the molecule as a result of the vibration caused by the absorption of infrared radiation. For

example, due to the difference in electronegativity between a carbon and oxygen atom, the

carbonyl group is permanently polarized. A stretching of this bond increases the dipole moment

and thus creates an characteristically intense band in an IR spectrum of acids, ketones,

aldehydes, and the like [4].

For ease of interpretation, vibrational frequency is converted to wavelength then inverted.

This unit of measurement is called a wavenumber (λ) and is denoted with units cm^{-1}. The IR

spectrum can be divided into three regions, the far infrared (400-0 cm^{-1}), the mid infrared (4,000-

400 cm^{-1}), and the near infrared (14,285-4000 cm^{-1}). Most applications utilize the mid-infrared

region as this contains the bulk of the molecular structural information. The near- and far-

infrared regions provide specialty information such as lattice vibrations; however, this

information is beyond the scope of this study. Within the mid-infrared region, the spectrum can

be further subdivided into four regions; X—H stretching (4000-2500 cm^{-1}), the triple bond

region (2500-2000 cm^{-1}), the double bond region (2000-1500 cm^{-1}), and the fingerprint region

(1500-400 cm^{-1}). It is the signals that appear in these regions which give the FTIR operator clues

as to the structure of the molecule being sampled [4-6]. A table of characteristic IR absorptions

for various chemical functional groups has been included in Appendix A.

2.1.3 IR Sampling Techniques

Collecting IR spectra via FTIR involves using one of the many sampling techniques which have been optimized to analyze specific materials. Sampling techniques can categorized into two subgroups: transmission methods and reflectance methods. Both sampling techniques are optimized for different types of samples. For example, a chemical solution is best contained in a transmission cell while it would be difficult to use that same configuration to collect IR spectra from a composite aircraft fuselage. Samples used in conventional transmission methods must first be small enough fit inside the sampling chamber and secondly must be thin enough to allow IR radiation to pass through the material and onto the detector on the other side.

Transmission spectroscopy is the oldest and most basic IR sampling technique. This method is based on the absorption of infrared radiation at specific wavelengths as it passes directly through the thickness of a sample. Using this approach it is possible to analyze samples in liquid, solid or gaseous forms. Many liquid and gas samples can be placed into a transmission cell of which there are several different configurations available. Fixed path length sealed cells, which are tightly sealed to prevent contamination or leakage, are useful for volatile liquids. Semi-permanent cells are demountable, allowing the technician to clean and re-use the cell. Figure 1 illustrates a typical semi-permanent cell used for the analysis of non-volatile solutions.

One characteristic common to all transmission cells is the presence of two windows, a front and back window used to contain the sample. As IR radiation must pass through this material, careful consideration must be made in choosing the type of window material used. This material must be transparent to IR radiation so as not to taint the sample spectrum. Alkali halides are normally used. Common materials include sodium chloride (NaCl) and potassium bromide (KBr) as they are inexpensive, readily available and transparent to incident IR radiation in the
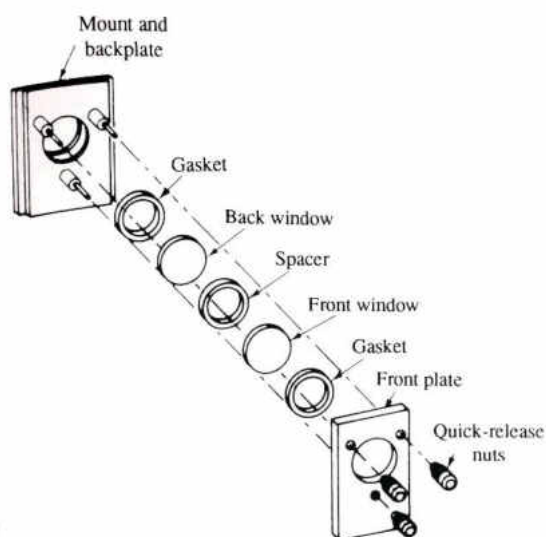
Figure 1: Schematic of semi-permanent cell. Used to analyze liquids [4].

mid-IR range. Some liquids can also be sampled as a film by placing a single drop between two

KBr plates which are then mounted into a simple spring-loaded cell holder. Solid samples can

also be prepared for analysis via transmission methods. Three geometries are used to analyze

solids: pellets, mulls, and films. The ground solid sample can be mixed into an alkali halide

(NaCl or KBr) and pressed into a pellet, mixed with mineral oil to form a mull, or cast into a thin

film which is then loaded directly into a cell holder [4].

Reflectance methods can be used for samples which are difficult to analyze with a

transmission cell and can be divided into two categories: internal reflectance and external

reflectance. Attenuated total reflectance (ATR) is a popular internal reflectance technique which

utilizes the phenomenon of total internal reflection. A beam of IR radiation entering a crystal will

undergo total internal reflection when the angle of incidence between the crystal and the sample

is greater than the critical angle. This can be easily achieved if the index of refraction of the ATR

crystal is significantly higher than that of the sample being tested. Properties of commonly used

crystals are summarized in Table 1. The IR beam penetrates a fraction of a wavelength beyond

the reflecting surface and when a material absorbs radiation, the beam loses energy. The resultant

Table 1: Materials commonly used as ATR crystals [4]

Crystal Material	Useful Range (cm^{-1})	Refractive Index	Properties
KRS-5	17,000-250	2.4	Soluble in bases; slightly soluble in water; insoluble in acids; highly toxic
ZnSe	20,000-500	2.4	Insoluble in water, organic solvents, dilute acids and bases
Ge	5,000-550	4.0	Insoluble in water; very brittle

attenuated radiation is measured and plotted as a function of wavelength yielding the IR

spectrum of the sampled material. Depth of penetration of the IR radiation into the sample is a

function of wavelength, refractive index, and the angle of incidence as seen in Eq. 4

$$d_p = \frac{\frac{\lambda}{n_1}}{2\pi \left[sin\theta - \left(\frac{n_1}{n_2} \right)^2 \right]^{0.5}} \tag{4}$$

where d_p is the depth of penetration, λ is the wavelength of light, n_1 and n_2 are the refractive

indexes of the two coincident materials and θ the angle of incidence. A typical depth of

penetration for an ATR configuration is between 2-5 microns [4].
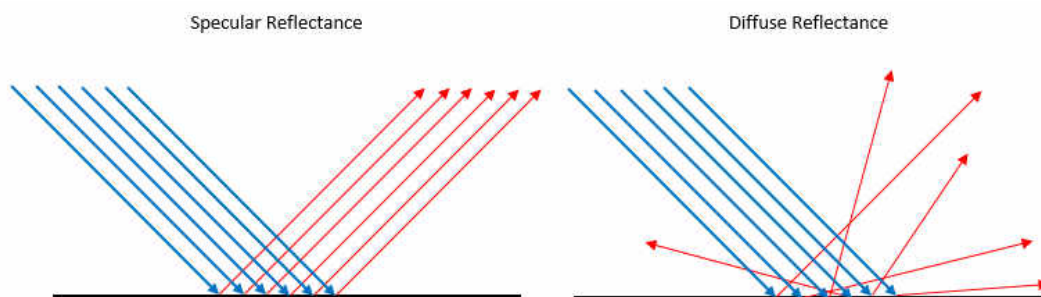

Figure 3: Representation of specular vs. diffuse reflectance

In external reflectance, incident radiation is focused on to the surface of the sample. Two forms of reflectance can occur: specular and diffuse. External reflectance measures the IR radiation reflected off the surface of the sample and therefore the material must itself be optically reflective or attached to a reflective backing plate. These methods are best used to study surface coatings, plated metals, and polymers. Specular reflectance occurs when the reflected angle of incident IR radiation equals the angle of incidence. The amount of light reflected back depends on a number of factors such as the angle of incidence, the refractive index, the sample's surface roughness, and the absorption properties of the sample. A sampling technique referred to as grazing angle (up to 85°) specular reflectance allows for the analysis of micro coatings. Lastly, the diffuse reflectance technique, commonly called DRIFTs (diffuse reflectance infrared Fourier Transform spectroscopy), analyzes the energy reflected back over a large angle after it has been scattered by a rough surface [4]. Figure 3 shows a representation of the difference between specular and diffuse behavior. This explains why specular reflectance FTIR units must be used with smooth samples and will not perform well on powders or samples with a rough surface finish.

2.2 Previous Work

Much work has been done to identify the cure states of thermosetting resins. Time-temperature-transition (TTT) diagrams of cure are created using a combination of differential scanning calorimetry (DSC), differential thermal analysis (DTA), and/or thermomechanical analysis (TMA). These diagrams are specific to the polymer being studied and present various cure states as a function of time and temperature [10]. As the polyester resin being examined in this study is of proprietary composition, a TTT diagram or tailored cure kinetics model is not

12

available. The following literature review will examine various methods for determining DOC without this information by validating DSC data with other methods spectroscopy techniques.

2.2.1 DSC/FTIR

With the advent of any new technique, time first must be spent validating its accuracy and precision. This validation has been accomplished by numerous researchers who have used methods such as differential scanning calorimetry (DSC) [3, 10-11] as well as electron spin resonance (ESR) spectroscopy [12] and ultrasound [13] to substantiate FTIR data. The use of FTIR brings many advantages over techniques such as DSC. While DSC has its advantages, it is largely limited as the data it records is solely the heat produced during a reaction. Research has shown FTIR spectra can be used to determine thermal properties [3, 10] but can also be used to provide clues to chemical composition and morphology allowing for the calculation of fractional conversions of polymer constituents [4-6, 11].

The cure kinetics of UP resins are complex as several reactive processes occur simultaneously. While many researchers have used DSC to measure isothermal cure kinetics of UP resins, details relating to the individual conversions of styrene and polyester have not been as widely explored. de la Caba *et al.* sought to study the reaction kinetics of the conversions of styrene and polyester C=C bonds using DSC and compared those results to a cure model developed for FTIR. Degree of cure was successfully calculated using DSC data and several methods found in literature. de la Caba *et al.* reported strong agreement of all four methods within the tested temperature range of 60°C-80°C. This data was then compared to the well-accepted autocatalytic model, Eq. 5-6, and once confidence was established that the data set was representative of the cure kinetics of the UP sample, it was compared to FTIR data collected [3]. The autocatalytic model calculates DOC as

13

$$\frac{dX}{dt} = kX^m(1-X)^n \tag{5}$$

$$k = A \exp(\frac{-E_a}{RT}) \tag{6}$$

where X is the overall degree of cure, m and n are constants, and k is the rate constant defined by the pre-exponential constant (A), activation energy (E_a), and the absolute temperature (T) [3].

The degree of cure of styrene and the polyester, both constituents of the UP resin, was measured by following the changes in the area of their characteristic C=C peaks. For the purpose of this study, an internal standard was also established, used to normalize the peak areas. The degree of cure was calculated for polyester and styrene with Eq. 7 and Eq. 8 respectively

$$X_{Polyester} = 1 - \frac{A_t(982\ cm^{-1})}{A_0(982\ cm^{-1})} \tag{7}$$

$$X_{Styrene} = 1 - \frac{A_t(912\ cm^{-1})}{A_0(912\ cm^{-1})} \tag{8}$$

where X is the overall degree of cure, A_t is the normalized absorbance at time t, and A_0 is the normalized absorbance at the start of the reaction. It was found that throughout the reaction the degree of cure of the polyester is higher than that of styrene. However, the difference between them decreases as time progresses. This is a result of a diffusion-controlled propagation reactions setting in. Towards the end of the reaction, the large polyester molecules are relatively immobile compared with the C=C units of the small styrene molecules. Thus the conversion of C=C polyester bonds is hampered while the conversion of styrene continues [3]. de la Caba *et al.* found that the degree of cure calculated using DSC fell between values calculated for styrene and polyester using FTIR with all three methods converging as time progressed to the final cure state [3]. It can be concluded that information obtained by FTIR is helpful in determining the degree of cure in a UP resin although more work needs to be done to identify and quantify the sources of discrepancy between FTIR and DSC during cure.

Pandita *et al.* sought to rectify the discrepancy between data produced by DSC and FTIR. To do this they modified a conventional DSC instrument to accept two custom-made fiber-optic probes which illuminated the sample and reference compartments of the DSC and returned the reflected light to a fiber-coupled FTIR spectrometer. In this way, DSC and FTIR data could be collected simultaneously. This configuration led to well-correlated data and was consistent with the autocatalytic model (within 5%) [11]. This study established the validity of FTIR as a thermal analysis technique. Many other researchers have gone on to validate FTIR using other methods [12-15].

2.2.2 Electron Spin Resonance and Ultrasound

Aside from conventional DSC techniques and simultaneous DSC-FTIR proposed by Pandita *et al.*, electron spin resonance [12], ultrasound [13], and dielectric-based techniques have all been used to study the cure kinetics of polymer resins. Scott *et al.* studied photopolymerization of a bisGMA/styrene blend and monitored its progression through various cure states using FTIR and electron spin resonance (ESR) spectroscopy. ESR is analogous to nuclear magnetic resonance (NMR) spectroscopy with the fundamental difference being that electron spins are excited instead of the spins of atomic nuclei, the subject of NMR. In the end, Scott *et al.* found a one-to-one agreement between data collected by ESR and FTIR which was substantiated using a prior study using photo-DSC. Scott was able to use both methods to determine the degree of cure in the bisGMA/styrene blend with varying blend compositions and isothermal cure temperatures [12]. ESR showed no advantages over FTIR in such an application.

Lionetto and Maffezzoli propose monitoring the cure of a thermosetting resin by measuring the velocity and attenuation of ultrasonic waves as they are sensitive to changes in viscoelastic characteristics of the resin. Researchers found that this method to be more sensitive

than conventional DSC or dielectric analysis as the ultrasonic wave propagation was able to detect changes in modulus during the vitrification stage when the cure reactions become diffusion controlled. In this stage of cure, the resin is nearly fully crosslinked and behaves like a glassy polymer, the remaining cure occurs over a very narrow range undetectable by DSC or dielectric methods. Furthermore the ultrasonic method was able to identify the onset of gelation with DSC level precision [13]. While promising, ultrasonic methods are limited by inadequate stability of conventional transducers at high temperatures and the need of a fluid coupling medium between the transducer and the material being tested. This coupling medium can change the shape of the waveform and thus affect the accuracy of the velocity measurement. An air-coupled ultrasound was proposed and tested by Lionetto and Maffezzoli however this produced noisy data which makes it difficult to qualify the method for precision applications [13].

2.2.3 Optical Methods

The newest trend in fiber-glass reinforced composite research is in optical sensing techniques. Evanescent wave spectroscopy (EWS) [14] and fiber Bragg grating [15] are two methods being used to monitor cure kinetics. Both methods take advantage of the unique optical properties of the E-glass fibers used to reinforce popular industrial composite materials and are designed to be performed *in-situ*. This means that data can be collected during production, while the composite part is being molded. Wang *et al.* proposes using a bundle of E-glass reinforcing fibers as a sensor for kinetic monitoring. This technique yields many advantages: (1) data can be collected *in-situ* allowing for real-time process monitoring; (2) the sensor can be used in either intensity or evanescent mode to obtain qualitative or quantitative data; (3) the fiber-bundle sensor does not disturb reinforcing fibers as there is no diameter mismatch; (4) these sensors can

also provide information regarding the interface chemistry between reinforcing fiber and surrounding matrix [14].

Wang *et al.* constructed a 6 cm sensor by bundling approximately 2500 individual filaments, polished the ends, and attached an SMA connector to either end. This sensor was then impregnated into a resin system and interfaced with an NIR-FTIR spectrometer to collect EWS spectra and a thermocouple used for calibration purposes. The research group found good correlation between traditional FTIR results and those produced using the fiber-bundle sensor. One downside of EWS is that analysis using the fiber-bundle sensor can only be conducted until the refractive index of the resin matrix approaches that of the E-glass sensor. This means that the progress of the reaction can only be tracked in real-time up to a certain point. In the case of the EPO-TEK 310M epoxy used in the study, data was obtained up to 60% cure of the epoxy [14]. This method yields unacceptable results for the purpose of our study as we are interested in the degree of cure as it approaches its final equilibrium state (>90%).

Aktas, Boyd and Shenoi took a different approach utilizing the optical properties of fiber-glass to create fiber Braff grating (FBG) sensors to monitor cure kinetics. A FBG sensor monitors the variation in the refractive index of the core of a single mode optical fiber. When light travels through a fiber, a narrow wavelength is reflected back, the center wavelength (λ_B) of this reflected band can be represented by the Bragg condition [15]

$$\lambda_B = 2n_{eff}\Lambda \tag{9}$$

where Λ is the period or spacing, and n_{eff} is the average refractive index over the length L of the grating. When the grating is subject to axial strain or when a temperature gradient is applied, the center wavelength of the reflected band will shift due to changes in pitch and the refractive index of the surrounding matrix. This means that a change in temperature can be correlated to the band

of reflected light in the optical fiber allowing researchers to monitor thermal changes as the resin cures [15]. Unlike EWS proposed by Wang *et al.* this sensor can be used over the entire cure cycle of the polymer. However, much like DSC methods, the FBG sensor does not provide any information regarding chemical composition or morphology. Instead, FBG simply provides a temperature history which can be used to deduce the extent to which the cure has progressed [15].

2.2.4 Applied FTIR

The United States Federal Aviation Administration (FAA) released a report in 2014 summarizing the research conducted to evaluate the Agilent 4100 ExoScan FTIR unit as a means of detecting thermal damage in aircraft composites. This handheld FTIR unit was developed for industrial use and introduced in 2008. Shortly after, the FAA in partnership with the University of Delaware, Sandia National Labs and The Boeing Company conducted a 3-year study to determine the value and feasibility of using this instrument for the analysis of composite-based aircraft components. Researchers studied the changes in IR spectrum after the epoxy resin composite materials were exposed to varying temperature and time levels. These results were then correlated to short beam shear data taken from the same population of samples [7].

Using specular and diffuse reflectance attachments for the Agilent 4100 ExoScan FTIR, researchers found that the quality of IR spectra diminished when fiber-rich regions of the composite were exposed in contrast to the resin-rich surface of the test coupon. With fiber-rich regions exposed, the diffuse reflectance attachment produced a spectrum with absorbance-to-noise ratios 2 to 3 times higher than the same sample under specular reflectance. Once it was understood how IR spectra responded to various physical properties of the sample, researchers

18

wanted to understand whether or not chemical changes at the surface of a composite part, as indicated by changes in IR spectra, are indicators of the sample's bulk mechanical properties [7].

Partial least squares was used to correlate IR and short beam shear data and a strong correlation ($0.76 < R^2 < 0.96$) was found between mechanical strength and chemical changes as indicated by FTIR. The research team then compiled this data into a database which was used to map the surface of a thermally damaged composite part [7]. This type of system becomes invaluable to aircraft maintaince technicians, for example, when evaluating lighting strike damage to a composite fuselage. A lighting strike leads to localized heating which could affect the composite and will need to be repaired. Knowing exactly where the damage is localized allows for complete and efficient patching of the plane. Once the repair is complete the system can also be used to validate the extent of the repair, ensuring all affected material was removed. Following the successful three year research project the Agilent 4100 ExoScan was written into the Boeing 787 Service Repair Manual to be used to evaluate thermal damage [7].

2.2.5 Summary

The above literature review provides a basis for the work presented in the following chapters of this paper. The work presented by de la Caba [3] and Pandita [11] shows that FTIR can be used to confidently calculate degree of cure which is of interest as this is a measure of the progress of the polymerization reaction with correlation to bulk mechanical properties [16-18]. FTIR is the method of choice for further research because the technology is portable and universal with sampling interfaces to accommodate many sample types. Additionally, FTIR is a non-destructive technique and affords the ability to test directly on the production part, a must for industrial applications.

CHAPTER THREE: MATERIALS AND TEST METHODS

3.1 Sample Fabrication

For this study a fiberglass-reinforced composite was fabricated using materials supplied

by LM Wind Power, a wind turbine blade manufacturer.

3.1.1 Fiber Reinforcement

The reinforcing fiber used in sample production was a unidirectional high modulus (HM)

glass with a woven strand mat backing. Fabric architecture is shown in Figure 4. While exact

material properties of this material are not available, the minimum desirable specifications are

listed in Table 2 as provided by LM Wind Power.

Table 2: Physical and mechanical properties of HM glass [19]

Attribute	
Fiber material	HM-glass
Average fiber density (without sizing)	2600 ± 20 kg/m^3
Average filament diameter	17 µm
Average elastic modulus	51500 ± 1000 MPa
Average tensile strength	≥ 1300 MPa
Average tensile elongation at break	$\geq 2.6\%$

3.1.2 Polymer Matrix

Polylite 413-575, also known as GT-125, is a polyester resin supplied by Reichhold Inc.

and was used as the matrix material to fabricate the composite sample plates. This is an

unsaturated polyester resin, meaning the monomer contains carbon-carbon double bonds or triple

bonds, such as those found in alkenes or alkynes, respectively. This resin is a thermoset formed
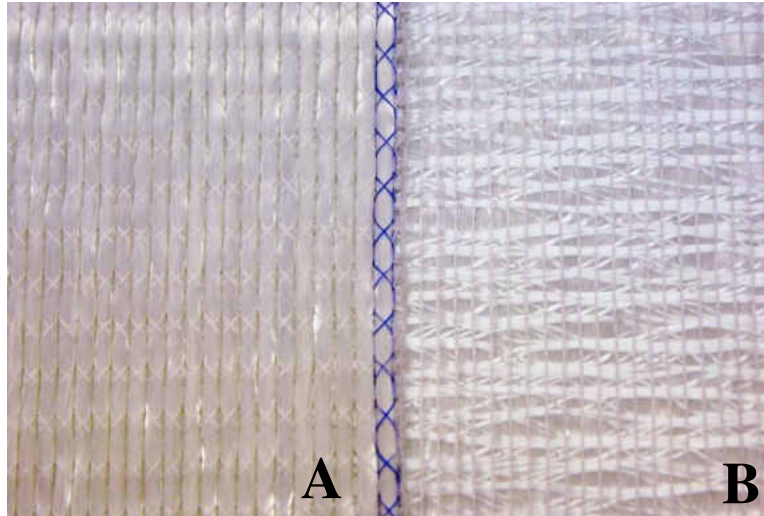
Figure 4: HM-glass with woven strand mat backing. (A) Clean side (B) Backing

through direct esterification of a diacid with a diol [20]. The polyester is then mixed with styrene, coloring agents and other additives to form the polyester blend resin. During production this blend is cured using one of many cross-linking techniques. In this particular instance, cross-linking is accomplished in a separate step by radical copolymerization with styrene, an alkene monomer. To do this, 1.5 wt% methyl ethyl ketone peroxide (MCP-75) is supplied to the blend as a free radical source to jumpstart the crosslinking reaction, weaving the polyester and styrene chains together to form a hardened polymer.

3.1.3 Vacuum Assisted Resin Transfer Molding (VARTM)

Composite plates used for testing were fabricated using a process known as vacuum assisted resin transfer molding, or VARTM. VARTM is a process which replaces one-half of a traditional two-part mold with a layer of vacuum bagging. Once a vacuum is created between the rigid mold and the vacuum bag, atmospheric pressure compresses the fiber package. Once the vacuum is stabilized, the resin infusion begins and any excess polymer is drawn out through an overflow vessel via the vacuum pump. This ensures that the final thickness of the production part is only as thick as the fiber package.

To fabricate large sheets of composite material, first a rigid aluminum work surface was covered with a thin layer of Meguiar's Mirror Glaze Mold Release #8 release agent. The fabric package consisting of six unidirectional HM-glass plies were stacked on top of the waxed surface. Plies were stacked with clean sides together at the mid-plane, alternating systematically with the backing facing outward on the outermost plies. This fabric package was then layered with several other materials to promote resin flow and provide easy removal of the composite plate from the vacuum mold. This process was completed per LM Wind Power control instructions. Table 3 lists the various layers and describes their purpose and Figure 4 shows a schematic of the fabrication set-up [21].

Table 3: Layers used in VARTM process

Layer	Purpose
Fabric Package	Constitutes the structure of the production part
Peel Ply	Provides a non-stick surface to easily remove the completed plate from the mold
Perforated Release Film	Serves as a breather to draw excess resin out and away from the fabric package
Perforated Plate	Distributes pressure evenly across surface of the fabric package during infusion
Infusion Net	Serves as a wick to draw the resin across the surface of the fabric package
Vacuum Bag/Tacky Tape	Creates a sealed package for infusion

Plastic spiral tubing is placed at the top and bottom of the fabric package. A solid line is used to draw the resin into the vacuum mold and spiral tubing distributes the resin across the length of the fabric. At the other end, more spiral tubing is used to collect excess resin out of the vacuum bag and into a second solid plastic line which delivers the resin to an overflow vessel. Once the entire assembly has been covered with vacuum bagging and sealed with tacky tape the vacuum pump is turned on to evacuate any air in the cavity. After any leaks have been fixed and the system reaches stability, infusion begins. Resin is allowed to flow through the fabric package
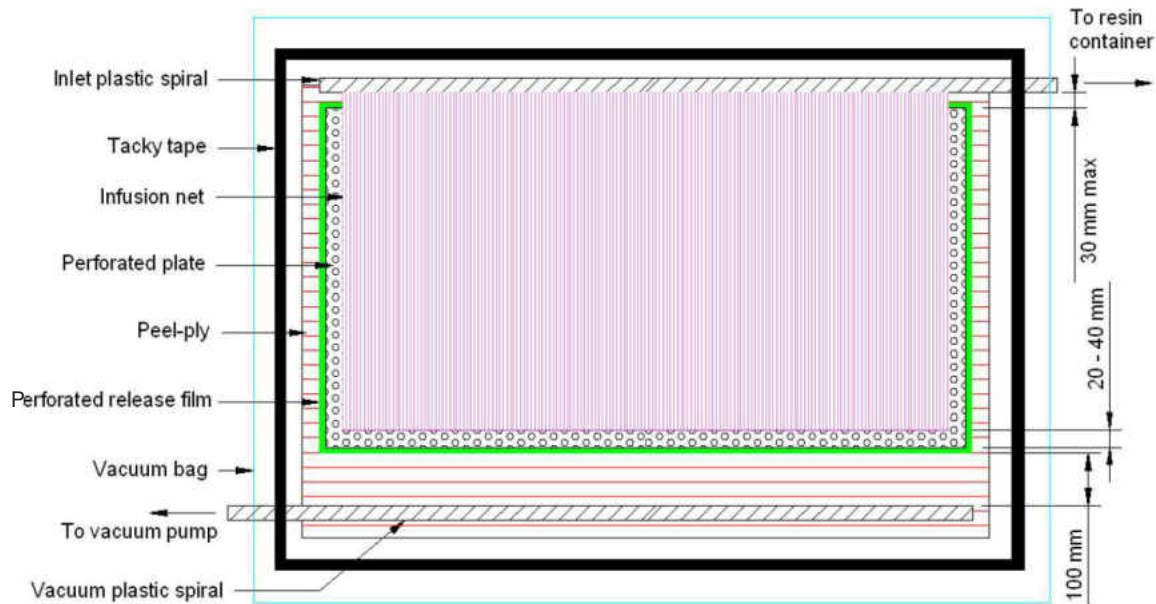
Figure 5: Diagram of VARTM fabrication set-up [21]

until the fibers have been completely saturated and excess resin begins flowing into the overflow vessel. At this point the vacuum is reduced to 60% and is maintained for a minimum of eight hours. After at least eight hours, the vacuum pump is turned off and the composite is allowed to cure at room temperature for an additional 8-10 hours at room temperature [21].

3.2 Identifying IR Bands of Interest

As the GT-125 resin contains an unknown polyester blend, it becomes advantageous to remove any dependencies of the analysis method on the polyester constituents and instead study the components of the resin which are known. This also allows the development of a robust method which can be used with other brands of unsaturated polyester resin. According to the material data safety sheet, GT-125 contains approximately 45 wt. % styrene, a common additive in polyester resins. Styrene is added to reduce viscosity but also enables the cross-linking of polyester chains without the evolution of any by-products [22].

de la Caba, *et al.* suggest calculating the degree of cure of an industrial unsaturated polyester resin using a peak at 912 cm^{-1} corresponding to C=C bonds present in the styrene monomer. While we can assume the composition of the resin used in de la Caba's study is similar, it must be verified that this peak is also present in our IR spectrum and also corresponds to the same styrene C=C bond. This can be achieved by monitoring a drop of GT-125 resin throughout its cure cycle and calculating the degree of cure based on formula suggested by de la Caba *et al.* [3].

To avoid damaging the Agilent 4100 ExoScan FTIR by placing the resin in contact with the ATR crystal a different approach was used to study the cure history of the liquid resin. A drop of initiated GT-125 resin was placed between two potassium bromide (KBr) sample plates and loaded into a Thermo Scientific Nicolet iS5 infrared spectrometer and outfitted with an iD1 transmission attachment. Figure 6 shows the sample before being loaded into the spectrometer. KBr is nearly transparent to IR radiation and thus allows us to collect an IR spectrum of only the polyester resin. An IR spectrum of the resin sample was taken approximately every 30 minutes throughout the 24 hour cure cycle.
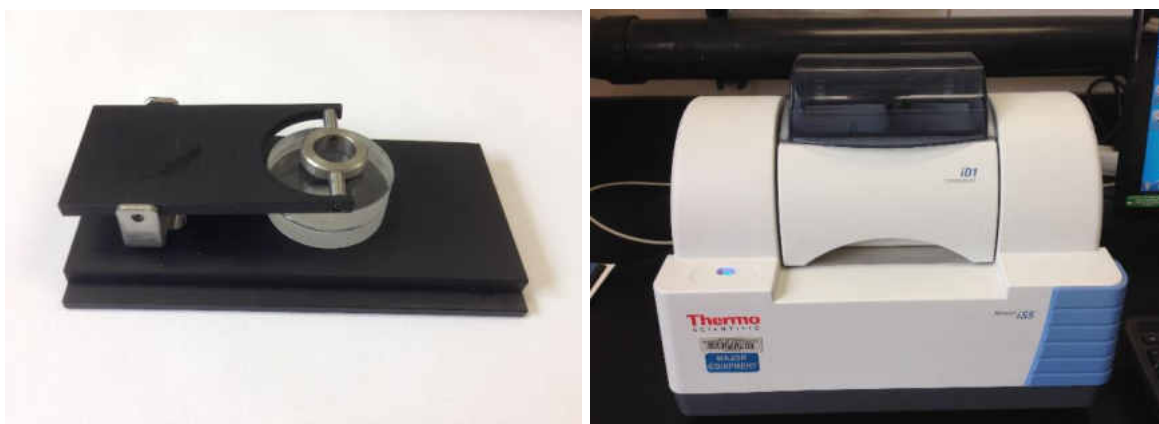

Figure 6: Nicolet iS5 and sample. (Left) Sample placed between two KBr plates (Right) Nicolet iS5 spectrometer with iD1 transmission attachment

Degree of cure (*X*) was calculated according to Eq. 10

$$X_{St} = 1 - \frac{A_t(912 \; cm^{-1})}{A_0(912 \; cm^{-1})}$$ (10)

where A_0 and A_t are the normalized absorbances before the reaction starts and after a certain time *t*. A C=O peak at 1722.8 cm⁻¹ was used as the normalizing parameter as the intensity of this peak does not change during the polymerization [3].
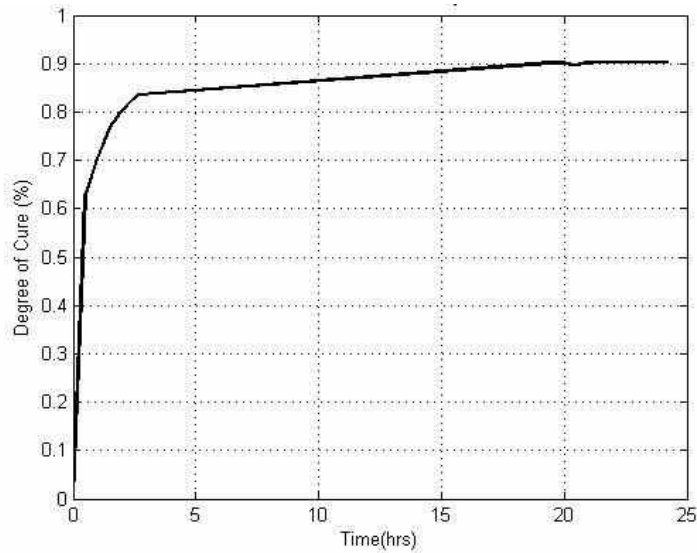

Figure 7: GT-125 cure history. GT-125/1.5 wt% MCP-75 liquid sample cured between two KBr plates and analyzed using Nicolet iS5 with iD1 transmission

Once cure stabilizes, after approximately 24 hours, a degree of cure vs time cure is produced. Figure 7 illustrates the progression of cure over the course of 24 hours. These values were calculated using Eq. 10 and the set of spectra in Figure 8. Notice the onset of maximum cure can be identified visually within the set of spectra as the styrene C=C peak at 912 cm⁻¹ stops changing signifying there are no longer C=C bonds left to dissociate. This process was repeated seven times and the data was used to qualitatively confirm two cure characteristics outlined in LM Wind Power literature. First, the GT-125 unsaturated polyester resin cure stabilizes at room temperature after 24 hours. Secondly, gelation occurs around the two-hour mark, consistent with the manufacturer's claim of a 125 minute gel time. Gelation signifies the irreversible
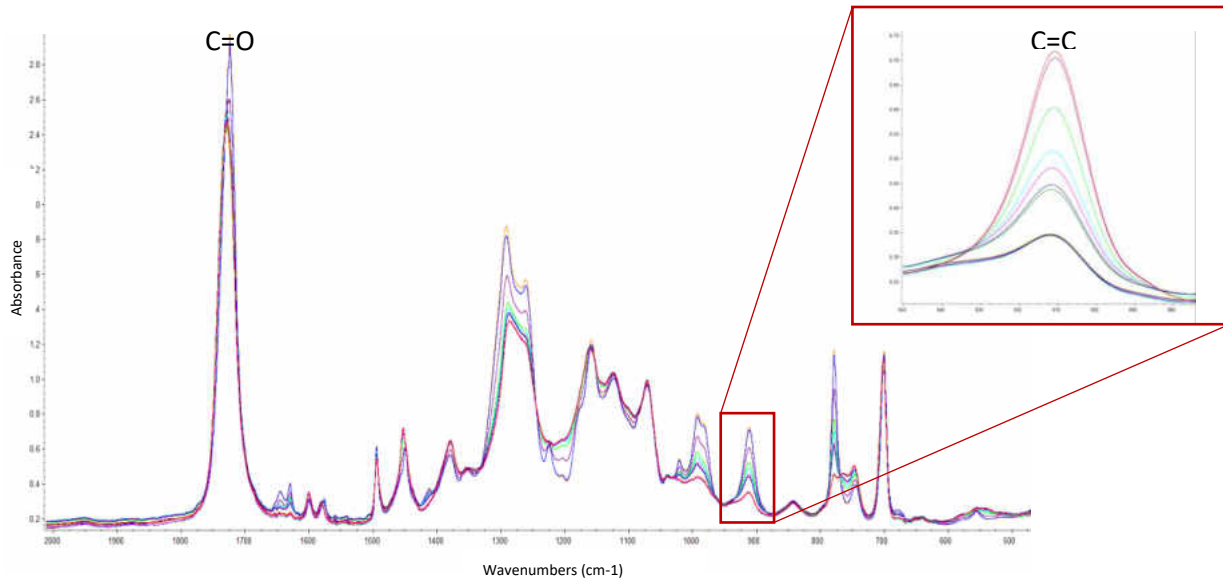
Figure 8: Spectral progression of cure in GT-125. Magnification emphasizing C=C peak at 912 cm⁻¹. GT-125/1.5 wt% MCP-75 liquid sample cured between two KBr plates and analyzed using Nicolet iS5 with iD1 transmission

transformation from a viscous liquid to a cross-linked gel. Past the gel-point, a thermosetting

resin is no longer capable of flow and is commonly defined as DOC = 80% [10]. Because these

observations match claims made by LM Wind Power, we can confirm our assumption that the

peak at 912 cm^{-1} corresponding to a styrene C=C bond is adequate in calculating the degree of

cure in our composite sample.

3.3 Attenuated Total Reflection (ATR) FTIR Spectroscopy

A series of samples cut from a single composite plate were analyzed using the Agilent

4100 ExoScan with the attenuated total refection (ATR) attachment, pictured in Figure 9. The

goal of this research is to evaluate ATR-FTIR as a means of determining the degree of cure in a

composite sample. This data will then be compared to a similar study completed using the

diffuse reflectance attachment for the Agilent 4100 ExoScan.

Figure 9: Attenuated total reflectance (ATR) attachment for Agilent 4100 ExoScan

3.3.1 Determining Effect of Sampling Parameters on IR Spectra

Before collecting data, a 2^4 full factorial design of experiment (DOE) study was conducted to analyze the effect of various sampling parameters on the quality of the resultant IR spectra. There are a number of sampling parameters which can be configured when using the Agilent 4100 ExoScan handheld unit. Many of these parameters are used to accurately translate the inferogram (raw data) into an interpretable IR spectrum with varying degrees of precision. These parameters are representations of complex processing algorithms which manipulate the raw data. These algorithms require processing power which ultimately determines the duration of time needed to complete the analysis of one sample. When needing to process hundreds of spectra for the purpose of academic research, time is a precious commodity so it must be determined how significant these factors are in affecting the spectrum's quality.

The response variable chosen was the signal-to-noise ratio (SNR). This variable provided a quantifiable measure of the IR spectra's quality. This metric becomes important during post-processing. A spectrum without noise allows for fewer prost-processing filters which need to be applied to ultimately calculate the degree of cure. Any manipulations to the raw data done during

post-processing add a level of ambiguity, or a source of error, to our data as an altered form of the spectrum is now being used to calculate the degree of cure.

A 2^4 full factorial design was implemented with two replicates (two blocks), and five center points per block. This resulted in a total of 42 runs, which although time consuming, yields the best possible design, free of aliasing. In design of experiments (DOE) aliasing is a negative product of an under sampled experiment where the estimate of a factor's effect also includes the influence of one or more effects, usually higher order interactions. The experimental design was generated randomly using Minitab 16. The goal of this DOE is to determine which sampling parameters effect the signal-to-noise ratio of the IR spectrum. Table 4 identifies the factors to be analyzed and the corresponding, high, low and center values. It is important to note that these are discrete factors, meaning sampling parameters are chosen from a list of pre-set values (i.e. cannot choose a resolution of 9 cm^{-1}, or a 4 pt smoothing algorithm) and the center value was not chosen as a numerical center but rather the option between the two extremes. To avoid the effect of an unusual observation, the experiment was run five times for each designated case and the mean signal-to-noise ratio was presented as the response variable.

Table 4: Factors considered to evaluate signal-to-noise ratio

Factor	Low (-1)	Center (0)	High (+1)
Number of Scans	4	16	64
Resolution (cm^{-1})	4	8	16
Apodization	None	Triangular	Happ-Genzel
Smoothing (pt)	0	5	7

Factors chosen to be analyzed are: the number of scans, resolution, apodization function and number of smoothing points. Each spectrum is a conglomerate of several individual interferograms. These multiple scans are averaged together and theoretically the more scans, or

interferograms, included in each spectrum the less sensitive the measurement is to noise. For example, if a particular functional group produces a very strong and defined peak then 4 scans may be enough because the peak will stand out no matter the amount of baseline noise. However, if a functional group has a very weak signal more scans will be necessary so that the peak has a chance to be seen through the random background noise. Resolution refers to the minimum peak interval that can be distinguished. The apodization factor refers to a mathematical function used to filter out leakage caused by the truncation of the interferogram at a finite optical path difference. Triangular and Happ-Genzel are two common apodization methods found in literature. It is important to note the apodization, while it helps to produce a smoother spectrum, does greatly affect the resolution. In practice, if optimal resolution is desired apodization should not be used. Happ-Genzel apodization accounts for approximately 50% loss in resolution. While this has no effect on simple chemistries and is often used to mitigate the effect of noise, the extent of apodization is of concern for complex molecules, especially in weak signal analysis. Lastly, the number of smoothing points refers to the number of successive points inputted to the Savitzky-Golay smoothing algorithm. This smoothing technique is based on a polynomial least-squares fitting. This particular smoothing algorithm is often chosen for FTIR application because, while it is less effective at reducing noise than a sliding-average approach, it is more effective in retaining the original shape of the signal [23].

Following the run order presented in Appendix B, Agilent MicroLab software was configured using the specified factor levels. Table 5 lists sampling parameters which remained unchanged throughout the course of the experiment. These parameters were of no interest in this particular application for a variety of reasons.

The spectral range denotes the range of wavenumbers of which the instrument will sample. In order to capture the entire IR spectrum, the default range of 4,000-650 cm^{-1} was used. Previous experimentation showed that in these operating conditions, i.e. ambient air, the number of background scans did not affect the quality of our spectra as our environment is relatively stable. If, for example, this experiment was conducted in an artificial atmosphere consisting of many make-up gases then the effect of the number of background scans would need to be taken into consideration. The zero fill factor refers to the amount of zero padding used to interpolate the inferogram. More zero fill produces a smoother spectrum but increases the number of points which make up the inferogram. The smoothing function was chosen over the zero fill method to maintain a consistent, and more directly comparable set of spectra. Lastly, Mertz phase correction is necessary to correct for out-of-phase elements which are introduced by optical path differences in the instrument. If this correction is ignored the resulting spectrum will not be an accurate representation of the sample. Therefore, it is important that this option remains engaged at all times [23].

Table 5: Sampling parameters to remain constant

Sampling Parameter	Set Value
Spectral Range (cm^{-1})	4,000-650 cm^{-1}
Number of Background Scans	16
Zero Fill Factor	None
Phase Correction	Mertz

Composite samples were mounted onto a 3D-printed sample holder which was rigidly affixed to the sample platform atop the 4100 ExoScan as seen in Figure 10. The sample holder ensured that the same geographical point on the sample was being sampled from one run to another.
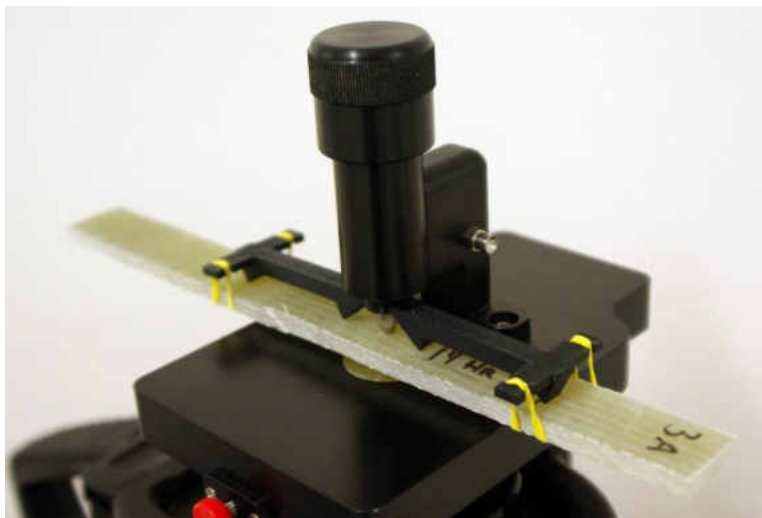
Figure 10: 3D-printed sample holder. Designed for use with ATR attachment.

Five samples were collected for each run. A software package called, eFTIR, software was used to perform the final smoothing process according to the experimental design table. Upon smoothing, each spectra was then processed with the same software and a signal-to-noise ratio was calculated using the noise band between 2700-2000 cm^{-1}. The average of the five data points was calculated and then input into Mintab 16; this average was used as the response variable.

After the average signal-to-noise ratio (SNR) was input as the response variable, Minitab 16 was used to analyze the full factorial model. Figure 11 shows a Pareto chart summarizing the statistical significance of each main effect and all higher-order interactions. It can be concluded that effect B (resolution) and effect D (smoothing) significantly affect the SNR, much more so than either the number of sample scans or the appodization algorithm used.

To confirm the validity of the collected data Figure 12 presents a normal probability plot and a residual versus fits plot. The normal probability plot passes the 'fat pencil test' with data points on either side of the fitted line ensuring the data is normally distributed. The residual versus fits plot illustrates no clear geometric pattern (i.e. cone or fishbone) and suggests no data

31

transformation is necessary. These plots assure the assumptions of a normal distribution and constant variance are valid for this experiment.

The results of this DOE show only two factors must be considered when addressing the issue of SNR, these are: sampling resolution (factor B) and the number of smoothing points used (factor D). Therefore we can safely minimize the number of scans taken per sample (time-intensive) and confidently omit the appodization parameter (computationally-intensive) to reduce the processing time of each spectrum. By doing this we can collect data points effectively and efficiently. This conclusion is supported by the interaction plots in Figure 13.
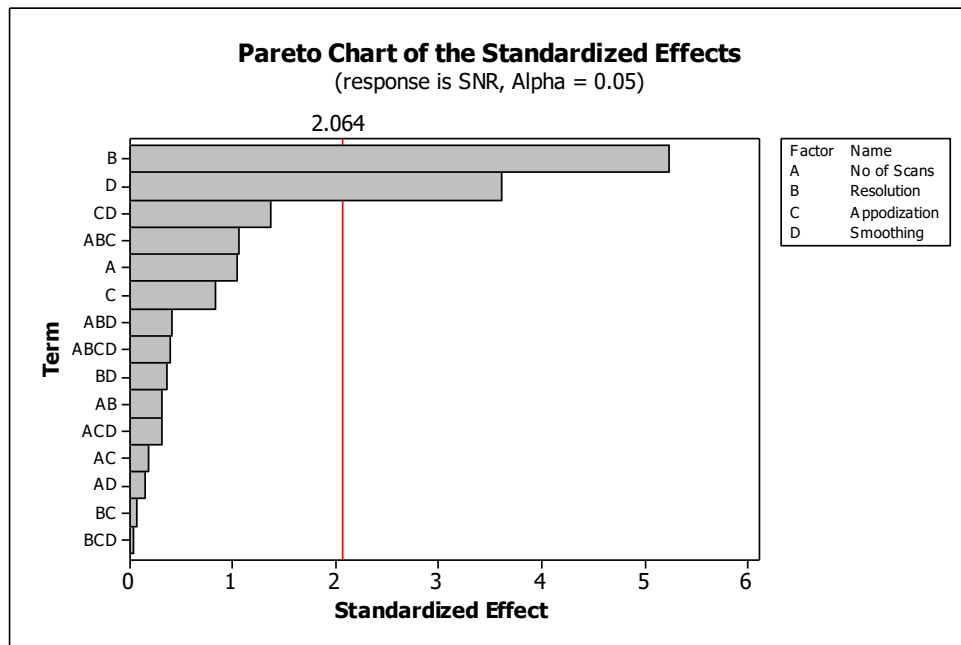
Figure 11: Pareto chart describing main effects of DOE. Shows that the resolution and number of smoothing points significantly contribute to the signal-to-noise ratio
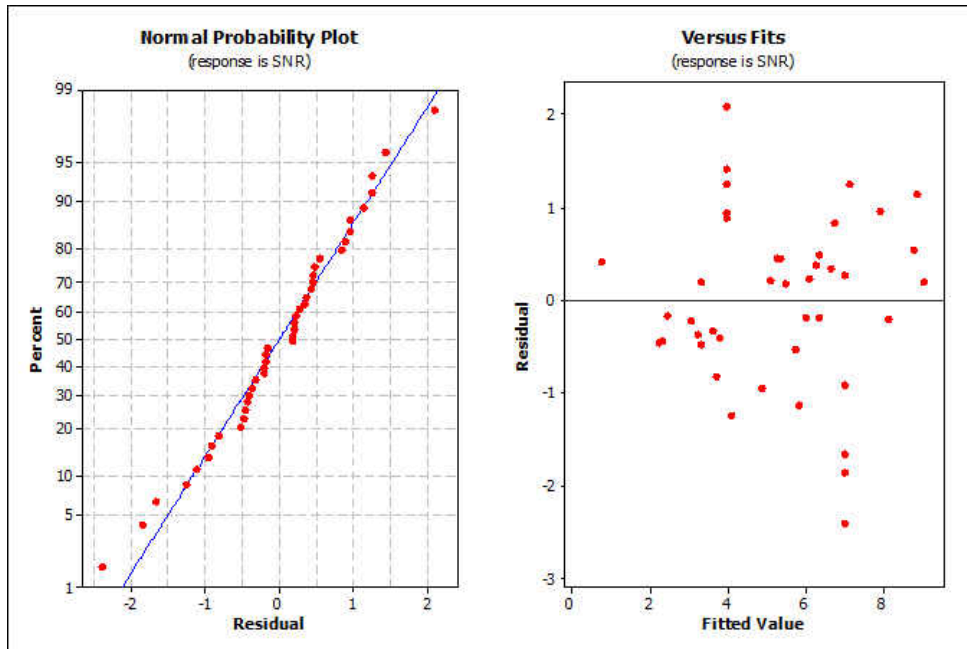
Figure 12: Normal probability and versus fit plots. (Left) Normal probability plot illustrates data set is normally distributed (Right) Residual vs fits plot illustrates no clear pattern, data transformation is not necessary
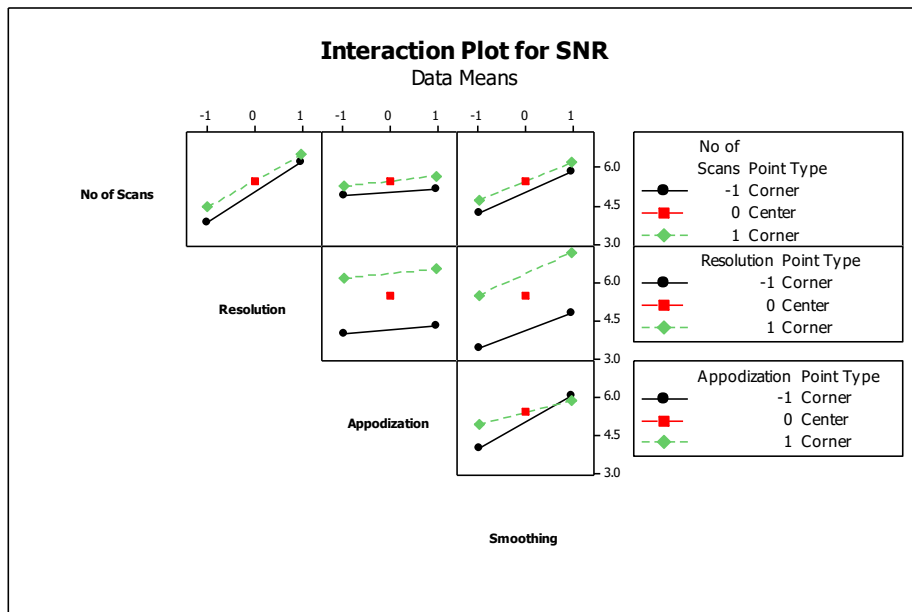
Figure 13: Interaction plot. Describes the dynamic relationships between factors. All interactions are mutually exclusive with the exception of appodization vs smoothing which shows relation

3.3.2 Configuring Agilent 4100 ExoScan for ATR

Based on the conclusions drawn from the full factorial experiment and suggestions

provided in Agilent operation manual, the FTIR unit was configured using the settings listed in

Table 6. Configuration of the Agilent 4100 ExoScan is achieved using the MicroLab PC companion software. Configuration profiles, called "methods", can then be saved and uploaded onto the handheld pc for future retrieval and use.

Table 6: Agilent 4100 ExoScan configuration settings for ATR

Factor	Setting
Method Type	Data Collect Only
Background	Collect New Background on Every Sample
Y-Axis Units	Absorbance
Spectral Range	Full
Background Scans	16
Sample Scans	32
Resolution	4 cm^{-1}
Zero Fill Factor	None
Apodization	HappGenzel
Phase Correct	Mertz
Sampling Technology	ATR

3.3.3 ATR Sample Preparation

All samples used in ATR analysis were cut from composite plates measuring 63.5cm x 38cm manufactured using vacuum assisted resin transfer molding (VARTM). A batch of resin consisting of 2,612.23g of GT-125 was mixed with 39.18g initiator, 1.50 wt%. The plate produced for this study consisted of 6 unidirectional HM-glass plies stacked in a symmetric fashion. A table saw outfitted with a diamond-tipped sawblade was used to cut the plates into 27cm long, 2.5cm wide strips with the fibers running the length of the sample. The plate yielded 15 samples.

Samples were placed in various post-cure environments to evaluate the effects of temperature history on the degree of cure. As the cure of the GT-125 is a thermal process, placing samples in a chest freezer will stop the reaction from proceeding, allowing the

preservation of the original cure state. Two samples were used as controls and allowed to cure at room temperature; they were used to evaluate the effectiveness of freezing the samples. Finally, three samples were placed in a convection oven for varying durations in attempt to drive the cure reaction to completion. Table 7 lists the various samples and their post-cure environments. This table summarizes the temperature history of each sample before being analyzed by ATR FTIR.

Table 7: ATR samples and corresponding post-cure environment

| Sample | Post-Cure Environment | | | |
	Stage 1	Duration	Stage 2	Duration
3A-1	Room Temperature (20°C)	1 Hr	---	---
3A-2	Room Temperature (20°C)	1 Hr	---	---
3A-3	Chest Freezer (-27°C)	24 Hr	---	---
3A-4	Chest Freezer (-27°C)	56 Days	---	---
3A-5	Chest Freezer (-27°C)	73 Days	---	---
3A-6	Chest Freezer (-27°C)	80 Days	---	---
3A-7	Chest Freezer (-27°C)	80 Days	---	---
3A-8	Chest Freezer (-27°C)	86 Days	---	---
3A-9	Chest Freezer (-27°C)	87 Days	---	---
3A-10	Chest Freezer (-27°C)	87 Days	---	---
3A-11	Chest Freezer (-27°C)	94 Days	---	---
3A-12	Chest Freezer (-27°C)	94 Days	---	---
3A-14Hr1	Chest Freezer (-27°C)	13 Days	Convection Oven (60°C)	14 Hr
3A-14Hr2	Chest Freezer (-27°C)	13 Days	Convection Oven (60°C)	14 Hr
3A-7Day	Convection Oven (60°C)	7 Days	---	---

3.3.4 ATR Sample Analysis

After the corresponding post-cure was achieved as discussed above, samples were analyzed using an ATR attachment on the Agilent 4100 ExoScan handheld FTIR. Frozen samples were first brought to room temperature for 20 minutes before FTIR analysis was performed. 60 consecutive spectra were taken once a day for 5 consecutive days. This produced a total of 300 spectra for each sample. Once pulled out of the freezer, the sample remained at room temperature for the duration of the test. Similarly, room temperature control samples were analyzed with the same frequency, 60 consecutive spectra per day, but for a longer window, a

total of 8 consecutive days. This was done to capture the full extent of the curing process from beginning to end. Lastly, samples placed in the convection oven were analyzed on a different schedule to attempt to capture the cure state before and after heating. 60 spectra were taken of 3A-14Hr1 and 3A-14Hr2 before being placed in the oven. After 14 hours, the samples were removed and 60 spectra were taken of each sample every 4 hours for a total of 240 spectra per sample. To further verify 14 hours was sufficient, 3A-14Hr2 was placed back in the oven at 60ºC for an additional 48 hours and 60 additional spectra were collected. For the 3A-7Day sample, 60 spectra were collected immediately after the 7 day post-cure and again 5 days later. This was done to verify that no additional curing occurred in the time the sample sat at room temperature once removed from the oven.

Spectra were taken at random over the entire length and width of the sample. Uniform pressure was applied during each scan with the help of a spring loaded sample mount supplied by Agilent. This was done with a set-up similar to what is pictured in Figure 10, but without the 3D-printed fixture used to constrain the sample in a single orientation.

3.4 Diffuse Reflectance FTIR Spectroscopy

Analysis showed substantial variation in the degree of cure calculated from samples using ATR. In attempt to rectify the noise introduced by the ATR method, a diffuse reflectance attachment for the Agilent 4100 ExoScan was also tested. Diffuse reflectance FTIR, commonly referred to as DRIFTs (diffuse reflectance infrared Fourier Transform spectroscopy) utilizes a much larger sampling interface than ATR. This means that a more representative spectra of the bulk material is produced by averaging the material's response to infrared over a larger interfacial area. DRIFTs also requires the use of a reference sample. For this study the included

Figure 14: (Left) Diffuse reflectance attachment (Right) reference sample cap for Agilent 4100 ExoScan

diffuse gold reference sample was used to calibrate for wavelength accuracy. Figure 14 shows

the DRIFTs configuration of the Agilent 4100 ExoScan with accompanying reference sample.

3.4.1 Configuring Agilent 4100 ExoScan for DRIFTS

The Agilent 4100 ExoScan was outfitted with the diffuse reflectance sampling interface

and a few minor changes to the instrument configuration were made to accommodate the new

sampling method. The configuration settings for DRIFTS can be found in Table 8. The most

notable change is the introduction of the method gain. The method gain is used to adjust the

intensity of the center burst, or the point at which the optical path difference is zero which

establishes a strong reference point. If this reference point is improperly set, then a weak signal

and noisy spectra will appear. In the case of the Agilent 4100 ExoScan, this intensity of the

center burst, or energy, must fall within a specified threshold before a resulting spectra is deemed

acceptable and the instrument will carry on with the analysis. It is important to note that this

value is dependent on the sample material and its surface finish. This method gain is set through

the "Advanced Features" menu in Agilent MicroLab PC.

Table 8: Agilent 4100 ExoScan configuration settings for DRIFTs

Factor	Setting
Method Type	Data Collect Only
Background	Background Valid Time Limit: 12 Hrs
Y-Axis Units	Absorbance
Spectral Range	Full
Background Scans	16
Sample Scans	32
Resolution	4 cm^{-1}
Zero Fill Factor	None
Apodization	HappGenzel
Phase Correct	Mertz
Sampling Technology	Reflectance
Sampling Subtype	Diffuse
Method Gain	235

A DOE was not performed as it was not yet clear whether or not the DRIFTs method would perform with similar, or better resolution, as ATR. Once it can be established that DRIFTs shows the potential for quantification, a DOE can be performed to optimize the sampling parameters and configuration settings to mitigate the effects of noise. Keep in mind the DOE was not performed as a method to establish time, temperature or cure state relationships of ATR spectra and was simply used to optimize processing parameters such as smoothing, appodization and resolution to produce the smoothest possible spectra for the analysis software.

3.4.2 DRIFTS Sample Preparation

For initial investigative research, resin coupons were fabricated using GT-125 polyester resin and 1.5 wt% MCP-75 initiator. The resin was poured into 1.5 inch diameter ring forms and allowed to cure. Buehler 20-8185-016 release agent was applied to the mounting table and ring forms for easy demolding and later removed with acetone before analysis. In the first batch of six samples, 3 were allowed to cure at room temperature for 7 days while 3 samples were cured in a convection oven at 60°C for 40 hours.

3.4.3 DRIFTS Sample Analysis

After the cure process was completed, the surface of the samples were first abraded on 120 grit silicon carbide sanding paper, supplied by Allied High Tech Products Inc., to remove any remaining surface residue from the sample. The energy threshold was not met if the abraded samples, regardless of sanding grit used, were placed directly on the sampling interface. Therefore, the computer would not allow the analysis to continue. In his book, Griffiths suggested the use of abrasive paper to transfer a small amount of material, creating a powder which would be analyzed more successfully by DRIFTS methods [6]. In attempt to replicate Griffiths' results the sample was then abraded to a second sheet of 120 grit sanding paper until the surface of the paper was saturated with powdered resin. The excess was tapped off and the sanding paper containing the powdered resin was placed on the Agilent 4100 ExoScan for analysis. Various grits of sanding paper were investigated but 120 was found to produce the smoothest IR spectrum with the least amount of interference. Figure 15 shows a comparison between a selection of three sanding papers considered. While the Allied High Tech 1200 grit provides a smooth spectrum, the high intensity peak occurring between 800-1,000 cm^{-1} would occlude the styrene C=C peak at 912 cm^{-1} leaving us with a spectrum which could not be quantified. The 3M sanding paper has a less intense peak which occurs between 800-1,000cm however, the curve does not have a stable baseline at higher wavenumbers. This would cause distortion in the C=O reference peak at 1722.8 cm^{-1}. The Allied High Tech silicon carbide 120 grit paper was chosen for its moderate intensity drop near 912 cm^{-1} and stable baseline at higher wavenumbers.
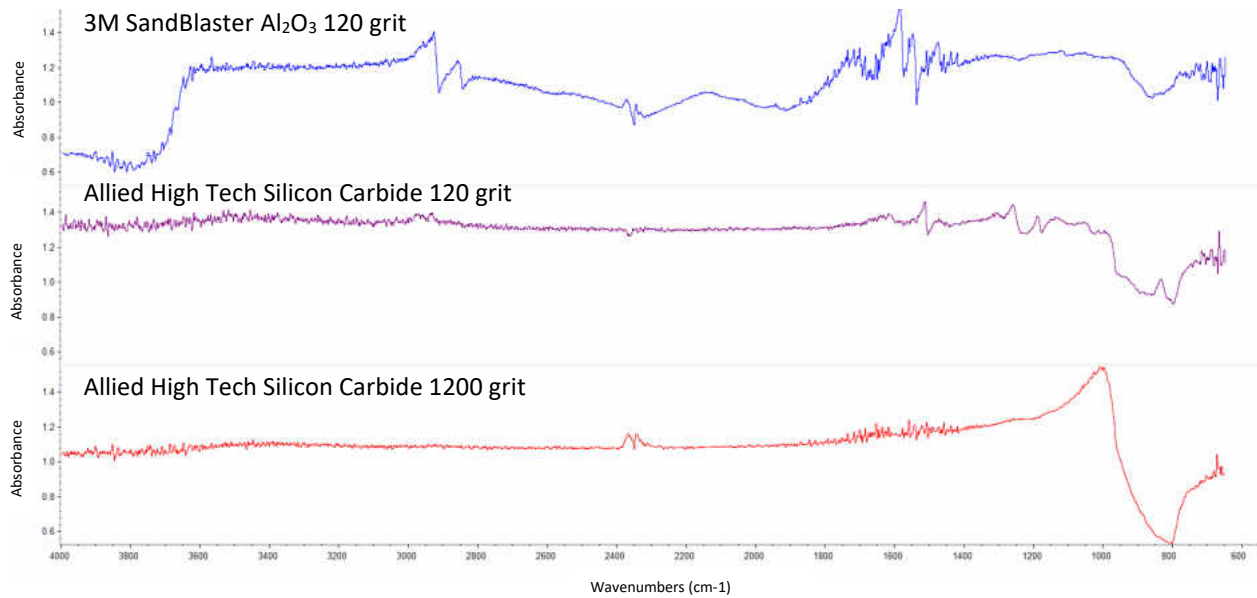
Figure 15: Spectral comparison of three sanding papers

Four spectra of each sanding paper were taken for each sample. All spectra were taken successively on the same day so that the cure state measured was not a factor of time but rather a factor of the post-processing method. The goal of this investigation was to determine if a change in cure could be seen between the two cure state extremes. Additional data would be needed to quantify degree of cure.

CHAPTER FOUR: RESULTS AND DISCUSSION

All data was gathered using the Agilent 4100 ExoScan and the software package provided by Agilent, MicroLab PC. These files were converted from the native Agilent .a2r format to .spc, a universal spectrographic data format using MicroLab PC. Quantification and further data processing was performed using a Thermo Fischer Scientific software package called OMNIC and a package distributed by Operant LLC called eFTIR. All analysis was performed using peak area, the convention in FTIR analysis. Peak height analysis as performed by eFTIR requires greater computational power than available as this software package does not allow the peak height analysis of individual peaks

4.1 ATR FTIR Results

Extensive work was done to quantify the degree of cure in the GT-125 polyester resin using ATR FTIR. The analysis of thousands of spectra led to important conclusions regarding the utility of such a device in monitoring the cure of an unsaturated polyester resin such as GT-125 in a manufacturing environment.

Due to the vast number of spectra collected during this portion of the study, OMNIC was first used to determine the integration limits on both the reference C=O peak at 1722.8 cm^{-1} and the styrene C=C peak at 912 cm-1. These integration limits are chosen by the software and are factors of spectral derivatives and baseline characteristics of the sample spectrum. Once these values were obtained, the spectra were batch processed using the Essential FTIR Spectroscopy

Toolbox (eFTIR), a 3rd party software distributed by Operant LLC. Simple integration to calculate the peak areas were performed using this software. This data processing method does lead to data points which need to be re-evaluated by hand as the spectrum may have excessive noise or a poor surface finish of the sample leads to a weak signal distorting the results. Only spectra which produced a negative peak area as given by eFTIR were re-evaluated by hand in OMNIC. Minitab 16 was used to plot the charts and graphs displayed in this section.

Figure 16 shows a representative spectrum of the GT-125 polyester resin as collected by ATR FTIR. If the HM-glass reinforcement fiber is exposed to the ATR crystal by means of sanding down the surface, the presence of the fiber can also be noted in the IR spectrum. The presence of the HM-glass fiber can be denoted by its distinctive O-H band. Care was taken to eliminate spectra containing this broad O-H band.
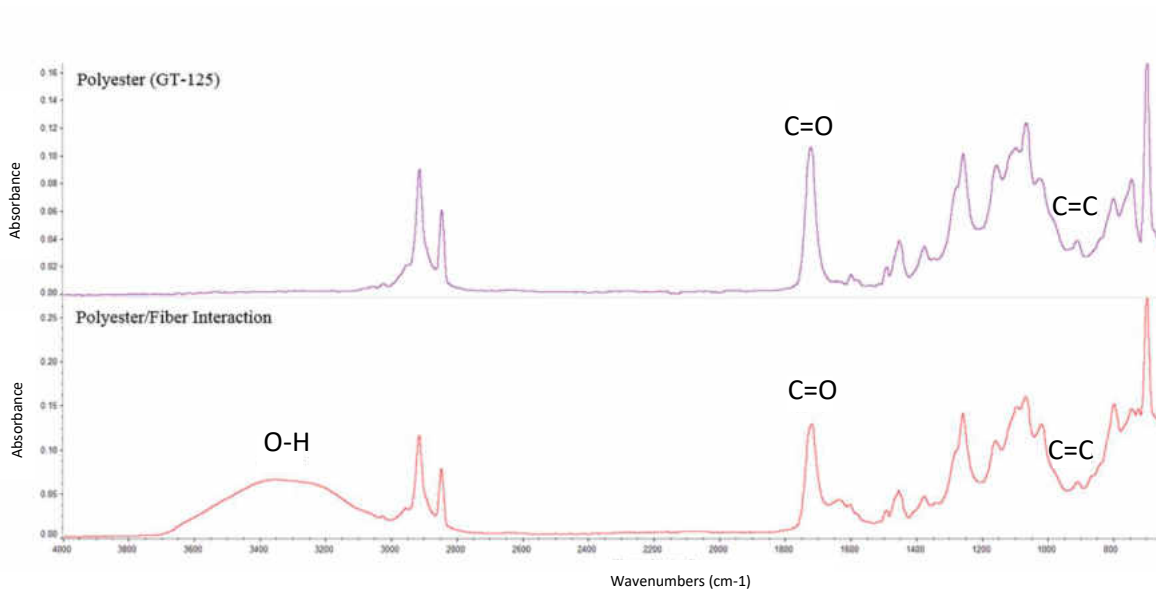
Figure 16: Effects of exposed HM-glass reinforcing fiber, broad O-H band

Examining the initial cure state of the ten samples placed in the chest freezer immediately after being cut we notice a wide range in calculated $A_t(912 \text{ cm}^{-1})/A_t(\text{Ref.})$ values for a given sample as seen in Figure 17 . As each one of the 60 individual spectra taken on each sample are
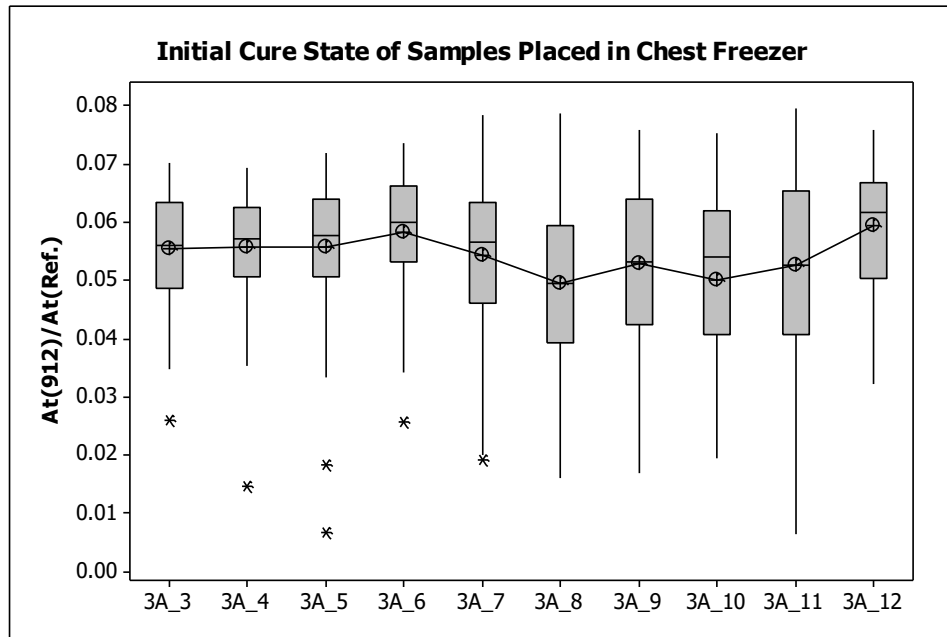
Figure 17 Comparison of the initial cure state of ten samples
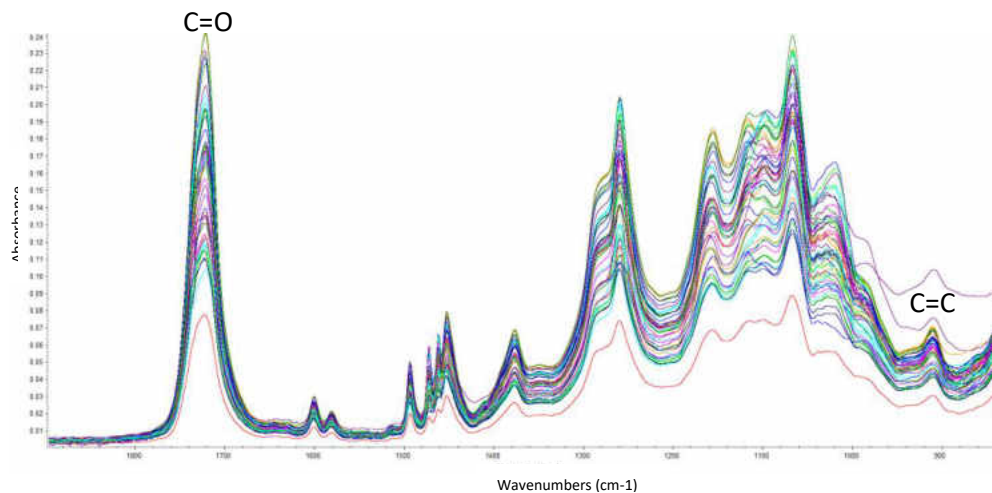
Figure 18: Sample 3A-3 at initial cure state

spread randomly over the length of the sample, the plot below suggests there is significant

variation in degree of cure from point to point. In addition it is also important to note as all ten

samples shown in Figure 17 underwent identical post processing and therefore should produce

similar results. Instead, each sample has a unique range and mean $A_t(912 \text{ cm}^{-1})/A_t(\text{Ref.})$ value.

This variation can also be seen when examining the spectra of these samples at their initial cure

state. For example, Figure 18 shows an overlay of all 60 spectra associated with sample 3A-3 at

the initial cure state as shown in Figure 18. First notice that in contrast to Figure 8 the C=O reference peak at 1722.8 cm^{-1} changes. While small variation is expected, this variation should change in direct proportion to the C=C peak at 912 cm^{-1} producing a consistent $A_t(912)/A_t(Ref.)$ value at any given time, t. Remember, the collection of spectra shown in Figure 18 was taken from the same sample and therefore should produce similar results regardless where FTIR analysis is being done on the sample. Upon further investigation, it becomes clear that this variation is not simply a function of sampling location but may also be a function of the background spectrum collected before each scan. Figure 19 shows an overlay of a series of spectra collected using the 3D-printed sample fixture discussed in the DOE portion. This series
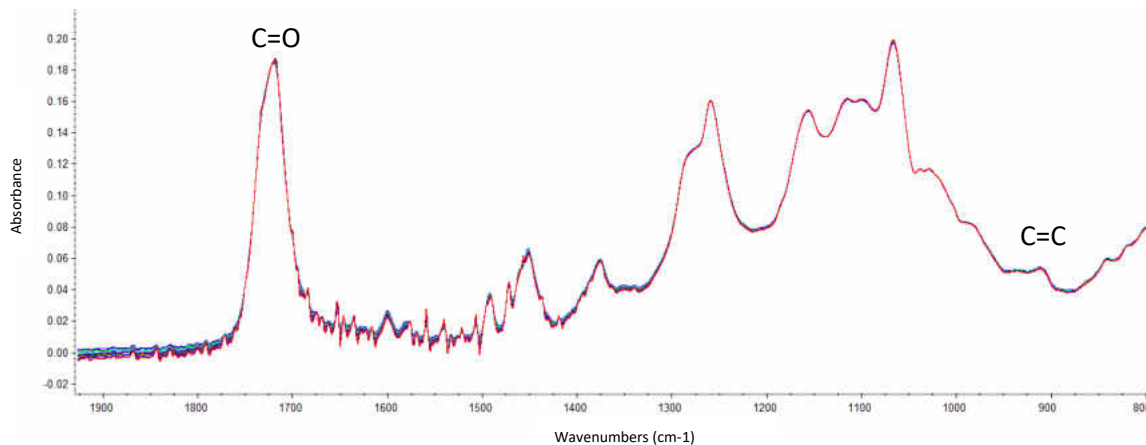
Figure 19: Overlay of ATR spectra evaluated for repeatability, single background reference
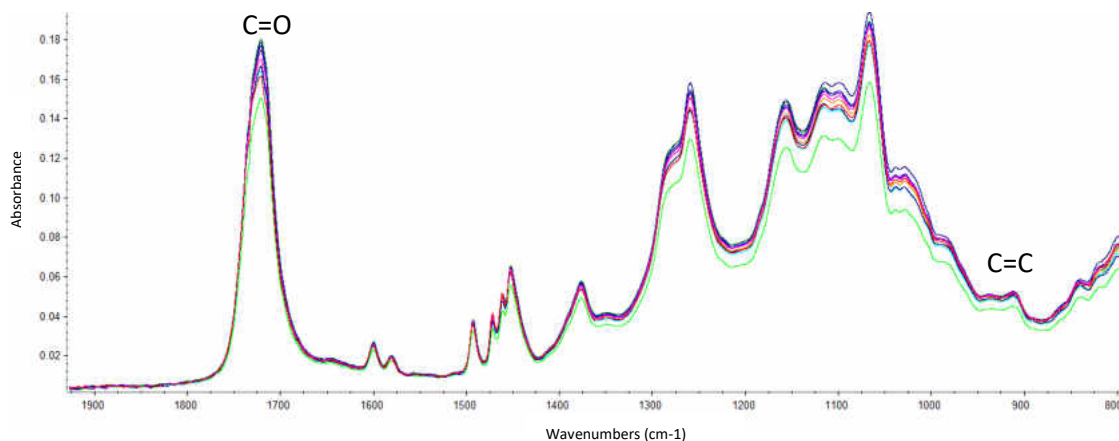
Figure 20: Overlay of ATR spectra evaluated for repeatability, update background reference

Table 9: Peak area for selected spectra

Spectrum	$A_t(912 \text{ cm}^{-1})$	$A_t(\text{Ref.})$	$A_t(912 \text{ cm}^{-1})/A_t(\text{Ref.})$
1	0.071	6.496	0.0109
2	0.070	6.552	0.0107
3	0.107	6.446	0.0166
4	0.081	6.477	0.0125
5	0.094	6.464	0.0145
6	0.090	5.468	0.0165
7	0.117	6.091	0.0192
8	0.101	6.232	0.0162
9	0.083	6.171	0.0135
10	0.104	5.5958	0.0186

of spectra references a single background spectra, taken before the first spectrum in the series is collected. In this configuration, the spectra line-up on-to-one with negligible deviation at both the C=O reference peak or the styrene C=C peak. Conversely, Figure 20 shows a series of spectra taken of the same sample but instead of referencing a single background spectrum, the background was updated after each run. This series of spectra also utilized the 3D-printed fixture to prevent the sample from moving with each successive scan. Note a substantial difference in the deviation at each target peak given this small change in the configuration of the Agilent 4100 ExoScan. To further show that these two peaks do not change proportionally to one another, Table 9 shows the peak areas calculated for the 10 spectra in Figure 20. Had these peak areas changed proportionally to one another the $A_t(912 \text{ cm}^{-1})/A_t(\text{Ref.})$ would remain consistent as this sample, 3A-14Hr1, is at a steady cure state.

To further investigate the utility of ATR FTIR in determining the degree of cure of a composite sample, a time history of $A_t(912)/A_t(\text{Ref.})$ was produced. Spectra for each sample were collected every 24 hours and the progression of cure can be seen as a decrease in $A_t(912)/A_t(\text{Ref.})$ over time which would result in an increase in DOC as calculated by Eq. 10.
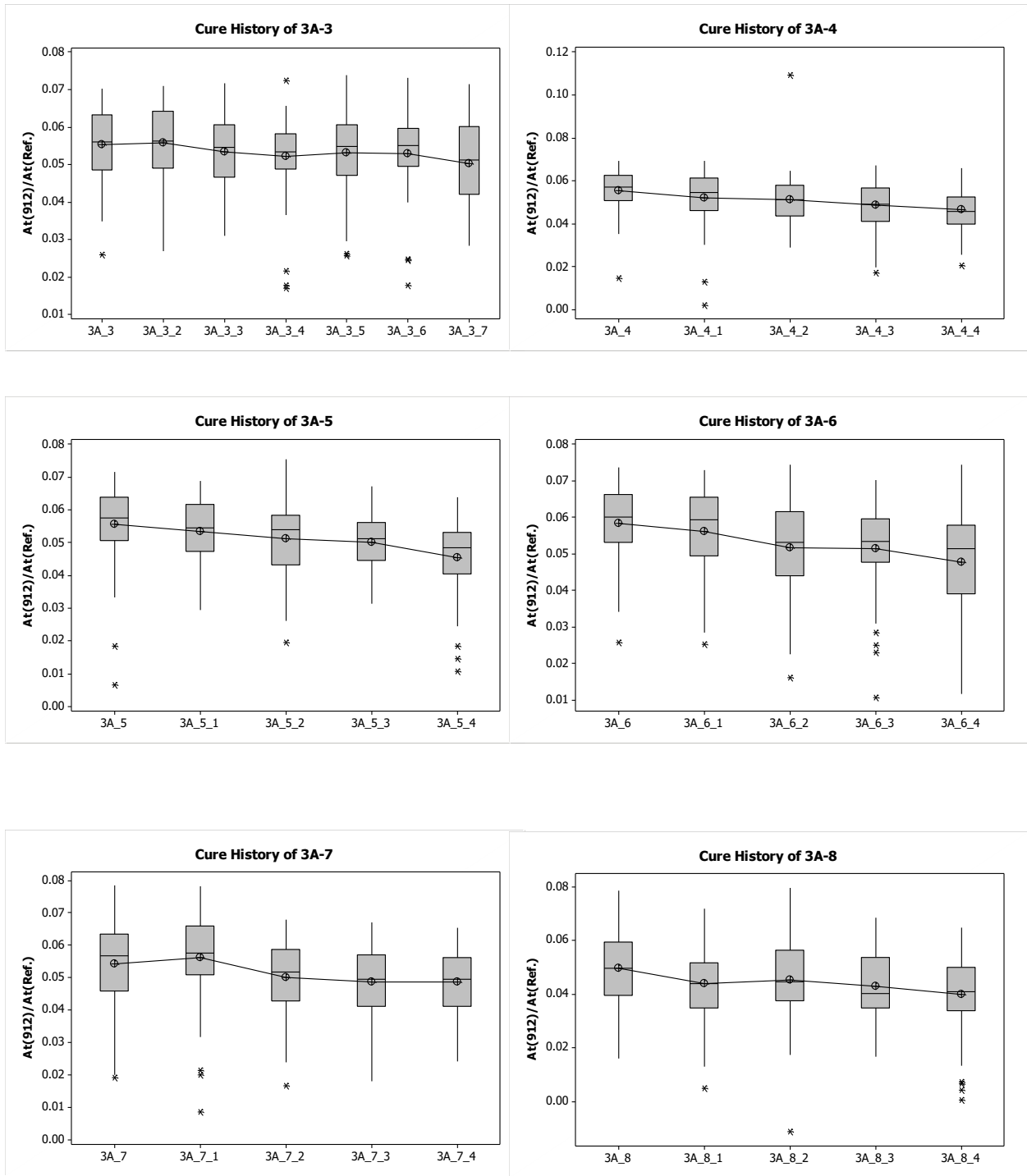
Figure 21: Cure histories for 10 samples

Figure 21 cont.
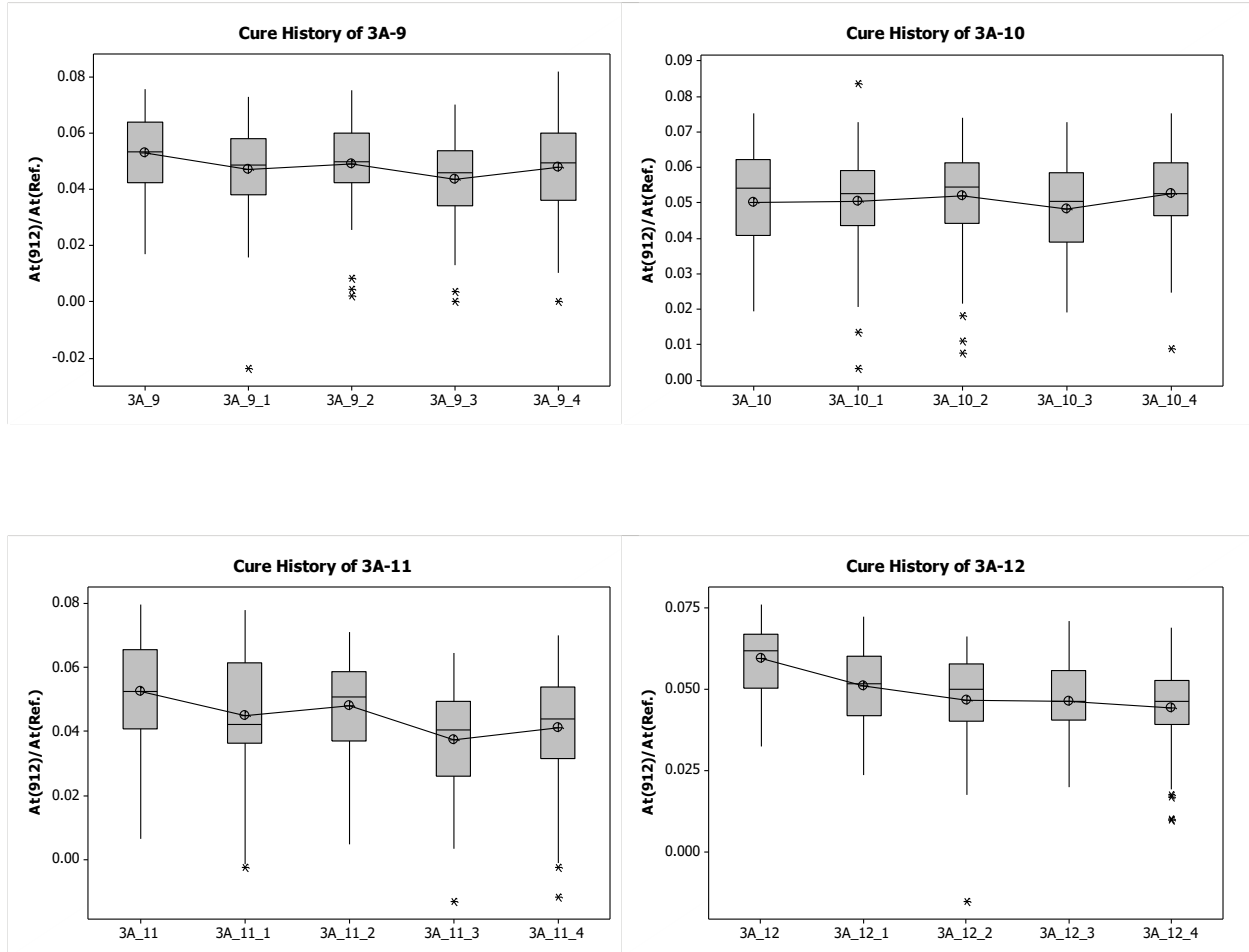
Figure 21: Cure histories for 10 samples

Due to the variation of $A_t(912 \text{ cm}^{-1})/A_t(\text{Ref.})$ values as noted above, calculating DOC no longer becomes meaningful. As noted in Eq. 10, DOC requires an initial cure state, if the mean value of each data set were to be used, individual data points may produces negative DOC values. For this reason, only $A_t(912 \text{ cm}^{-1})/A_t(\text{Ref.})$ values are presented.

While many of these samples behave in the expected manner, as presented in Figure 21, the wide range in observed $A_t(912)/A_t(\text{Ref.})$ values introduces a level of uncertainty which makes it difficult to quantify the DOC with an acceptable level of confidence. This can be
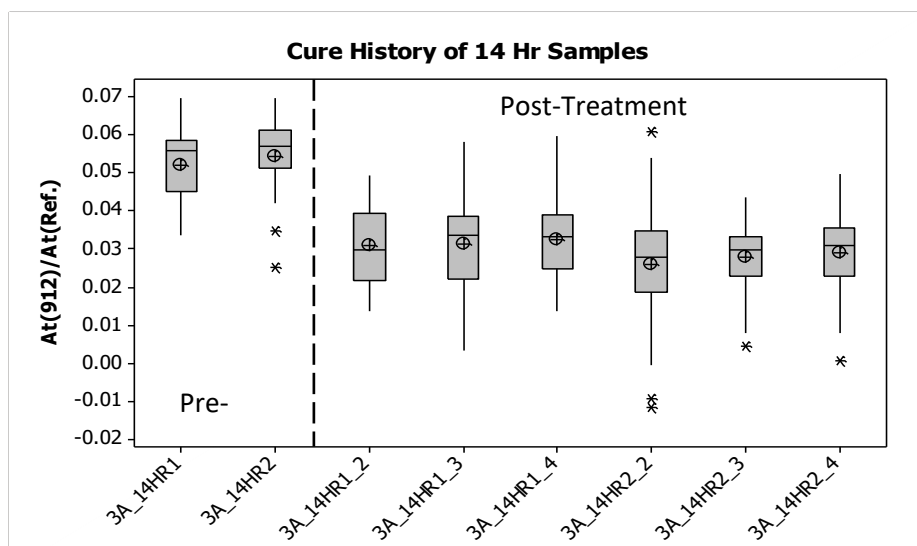
Figure 22: Comparison of $A_t(912)/A_t(Ref.)$ pre- and post-treatment. in samples 3A-14Hr1 and 3A-14Hr2

illustrated more clearly when examining the difference in $A_t(912)/A_t(Ref.)$ values calculated from spectra taken just before, and just after, post-cure treatment in the convection oven. Figure 22 shows the mean value in these two instances in the 3A-14Hr1 and 3A-14Hr2 samples are distinctly, different. However, considering the entire range of spectra collected of each sample, an entire quartile of data falls within the range denoted by the two samples at their pre-fired state. To determine a level of statistical significance, 95% confidence intervals around the mean $A_t(912 \text{ cm}^{-1}))/A_t(Ref.)$ value are constructed. These confidence intervals provide a measure of uncertainty as a result in the variation in our data. The confidence interval states that 95% of the time a subsequent sampling of data, taken under identical conditions, with mean X will fall within the given range. Looking at Table 10 we can say with 95% confidence these two cure states, as described by ATR FTIR data, are statistically different. This is because the mean value for 3A-14Hr1 and 3A-14Hr2 fall well outside of the confidence intervals established for subsequent post-cured samples. In addition, this data suggests that samples fired for 14 hours at 60ºC were not cured completely as the mean value for 3A-7Day falls outside the confidence interval for 3/6 post-treated data sets listed in Table 10.

Sample Index	Mean $A_t(912 \text{ cm}^{-1})/A_t(\text{Ref.})$	95% Confidence Interval (Mean)
3A-14Hr1	0.05180	(0.04771, 0.05589)
3A-14Hr1-2	0.03094	(0.02822, 0.03365)
3A-14Hr1-3	0.03134	(0.02845, 0.03423)
3A-14Hr1-4	0.03246	(0.02995, 0.03498)
3A-14Hr2	0.05435	(0.05003, 0.05867)
3A-14Hr2-2	0.02567	(0.02181, 0.02953)
3A-14Hr2-3	0.02790	(0.02561, 0.03020)
3A-14Hr2-4	0.02872	(0.02606, 0.03139)
3A-7Day	0.02725	(0.02352, 0.03098)

To relate this back to the cure histories presented in Figure 21, a similar confidence interval table has been created as seen in Table 11. By noting the frequency a mean $A_t(912 \text{ cm}^{-1})/A_t(\text{Ref.})$ value falls below the lower bound of preceding confidence intervals a time-based resolution can be established. For example, the 3A-4 series shows statistical significance after 24 hours but all spectra taken after that point do not have a mean value statistically significant than the previous day's data set. Reviewing other data series, it is clear there is no common trend and therefore a time-based resolution cannot be established at a 95% confidence interval.

Table 11: Comparison of 95% confidence intervals for 3A series samples as determined by 1-sample Z-test

Sample Index	Mean $A_t(912 \text{ cm}^{-1})/A_t(\text{Ref.})$	95% Confidence Interval (Mean)
3A-3	0.05535	(0.05277, 0.05794)
3A-3-2	0.05580	(0.05317, 0.05843)
3A-3-3	0.05344	(0.05074, 0.05613)
3A-3-4	0.05228	(0.04949, 0.05507)
3A-3-5	0.05327	(0.05030, 0.05624)
3A-3-6	0.05304	(0.05016, 0.05592)
3A-3-7	0.05037	(0.04637, 0.05436)
3A-4	0.05561	(0.05326, 0.05795)
3A-4-1	0.05192	(0.04884, 0.05400)
3A-4-2	0.05128	(0.04843, 0.05412)
3A-4-3	0.04858	(0.04591, 0.05125)
3A-4-4	0.04657	(0.04415, 0.04899)
3A-5	0.05576	(0.05279, 0.05873)
3A-5-1	0.05343	(0.05090, 0.05595)

3A-5-2	0.05139	(0.04868, 0.05410)
3A-5-3	0.05016	(0.04809, 0.05222)
3A-5-4	0.04561	(0.04282, 0.04840)
3A-6	0.05841	(0.05580, 0.06102)
3A-6-1	0.05608	(0.05317, 0.05899)
3A-6-2	0.05180	(0.04877, 0.05483)
3A-6-3	0.05133	(0.04837, 0.05428)
3A-5-4	0.04774	(0.04453, 0.05094)
3A-7	0.05427	(0.05122, 0.05733)
3A-7-1	0.05621	(0.05095, 0.05760)
3A-7-2	0.04998	(0.04729, 0.05268)
3A-7-3	0.04875	(0.04594, 0.05156)
3A-7-4	0.04859	(0.04636, 0.05082)
3A-8	0.04949	(0.04628, 0.05271)
3A-8-1	0.04381	(0.04051, 0.04710)
3A-8-2	0.04517	(0.04162, 0.04873)
3A-8-3	0.04289	(0.03979, 0.04599)
3A-8-4	0.03982	(0.03622, 0.04341)
3A-9	0.05291	(0.04958, 0.05623)
3A-9-1	0.04695	(0.04302, 0.05089)
3A-9-2	0.04917	(0.04535, 0.05299)
3A-9-3	0.04372	(0.04018, 0.04726)
3A-9-4	0.04781	(0.04368, 0.05194)
3A-10	0.05016	(0.04668, 0.05364)
3A-10-1	0.05045	(0.04697, 0.05393)
3A-10-2	0.05212	(0.04859, 0.05565)
3A-10-3	0.04813	(0.04485, 0.05140)
3A-10-4	0.05246	(0.04939, 0.05553)
3A-11	0.05260	(0.04864, 0.05656)
3A-11-1	0.04507	(0.04039, 0.04975)
3A-11-2	0.04791	(0.04426, 0.05155)
3A-11-3	0.03754	(0.03361, 0.04147)
3A-11-4	0.04116	(0.03680, 0.04551)
3A-12	0.05941	(0.05708, 0.06174)
3A-12-1	0.05083	(0.04778, 0.05388)
3A-12-2	0.04644	(0.04266, 0.05022)
3A-12-3	0.04632	(0.04328, 0.04935)
3A-12-4	0.04431	(0.04121, 0.04742)

The data above shows that statistical significance cannot be determined for samples between 24-120 hours after infusion using the styrene C=C peak at 912 cm^{-1} and the C=O reference peak at 1722.8 cm^{-1}. In attempt to establish a set of peaks that does show a trend and establish statistical significance on this time frame, various other peaks were analyzed using the eFTIR software. Table 12 lists the sample and reference peaks analyzed. These peaks were chosen because they had consistent limits of integration, meaning the peaks did not shift from one spectrum to another. In addition, the intensity of absorbance in the sample peaks exhibited fluctuation and did not remain relatively stable as did the peaks chosen as references.

Table 12: Sample and reference peak combinations for analysis

Sample Peak (cm^{-1})		Reference Peak (cm^{-1})
697.7		1722.8 (Ref.)
912.0		2913.6 (Ref. 1)
1214.9-947.0		1722.8 (Ref.)
1259.6		1722.8 (Ref.)
1259.6		2845.4 (Ref. 2)

Reviewing the resulting histories presented in Appendix C, it is clear there are no observable trends in any of the five peak combinations. Furthermore, the reference peak, Ref. 1, cannot be considered a stable reference as it alters the cure histories of the styrene C=C peak, meaning the two peaks do not change in proportion to one another, or the noise of the calculated peak area is too large and occludes any underlying trend.

Based on the presented data, it can be concluded that ATR FTIR can only be used to identify differences in cure state at 95% confidence when that composite is subjected to one of two extreme states: freshly demolded (approx. 24 hours after infusion begins) or a post-treated (additional 14 hours at elevated temperature, 60°C). In addition, there is evidence that the recommended post-cure of 14 hours at 60°C is not sufficient in driving the polymerization reaction to completion. Change in the cure state was observed after comparing 14 hour cured

samples with a sample which was cured for 7 days at 60°C. Due to the statistical spread in the calculated $A_t(912\ \text{cm}^{-1}\ )/A_t(\text{Ref.})$ values it becomes difficult to quantify DOC as information of an initial cure state is needed. Therefore we cannot with any certainty provide a discrete quantification of DOC at the two aforementioned cure states, however; statistical analysis shows us that we can say with 95% confidence, there is some difference as described by the data collected using ATR FTIR under the discussed sampling conditions.

4.2 DRIFTS Results

The work conducted with the diffuse reflectance attachment was exploratory in nature and for this reason quantification was not performed. Rather a qualitative review of the collected spectra will be conducted.

Figure 23 shows a representative analysis of the Allied High Tech 120 grit sanding paper with GT-125 powder cured at room temperature. This can be contrasted to a similar sample collected using ATR as seen in Figure 16. When overlaid with a spectra of the clean sanding paper it is clear, as seen in Figure 24, the effect the paper plays in determining the shape of the sample spectra. This is because absorbance is communitive in nature. While it can be assumed
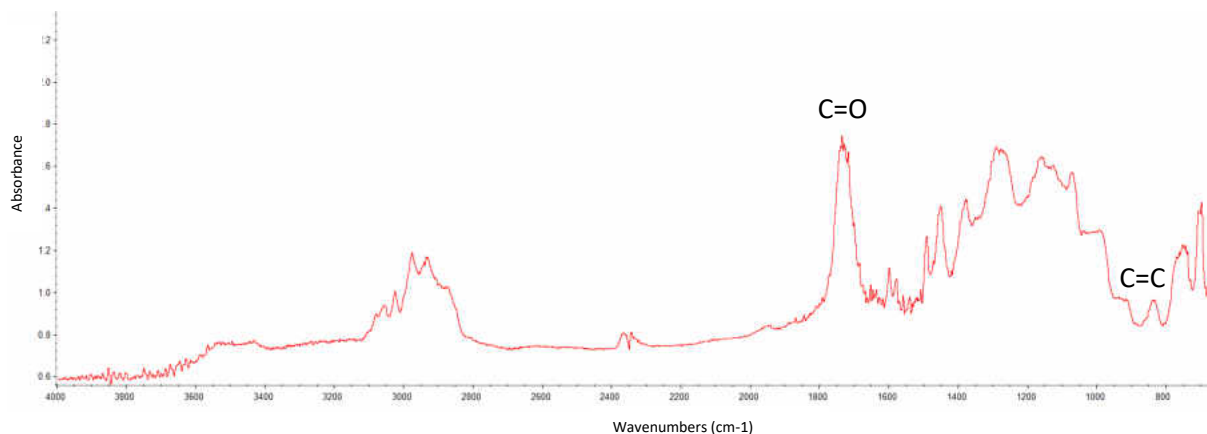
Figure 23: GT-125 (room temperature cure) on Allied High Tech silicon carbide 120 grit sanding paper
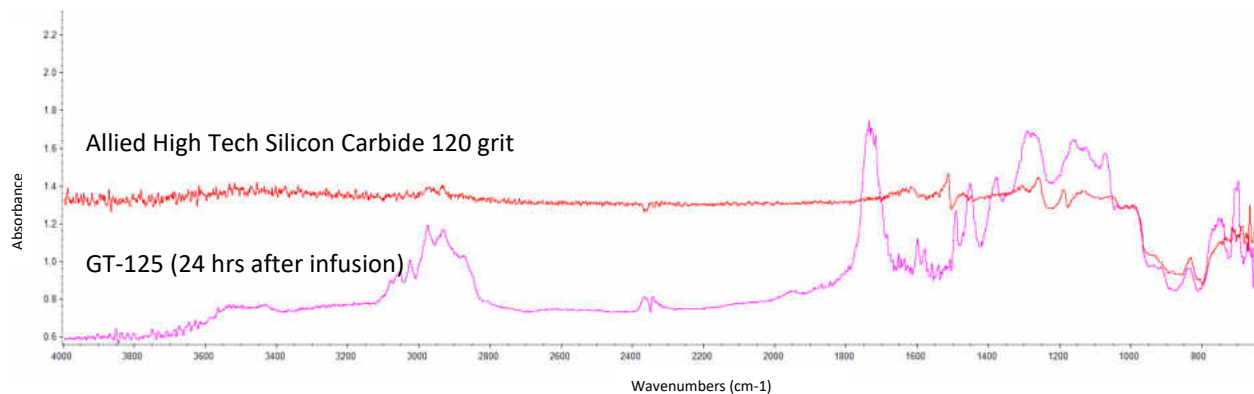
Figure 24: Sanding paper and GT-125 spectra overlaid

that the intensity drop near 950 cm^{-1} in the sanding paper spectrum occludes weak signals in the sample spectrum it is clear a discernable peak appears in our region of interest, at approximately 912 cm^{-1}. The presence of this peak would allow for the quantification of degree of cure using the methods described earlier.

To further determine if a notable difference in the DRIFTs spectra between freshly demolded and post-cured samples exists, the spectra were further processed in OMNIC. Figure 25 shows a conglomeration of all the spectra collected for this portion of the study. These spectra
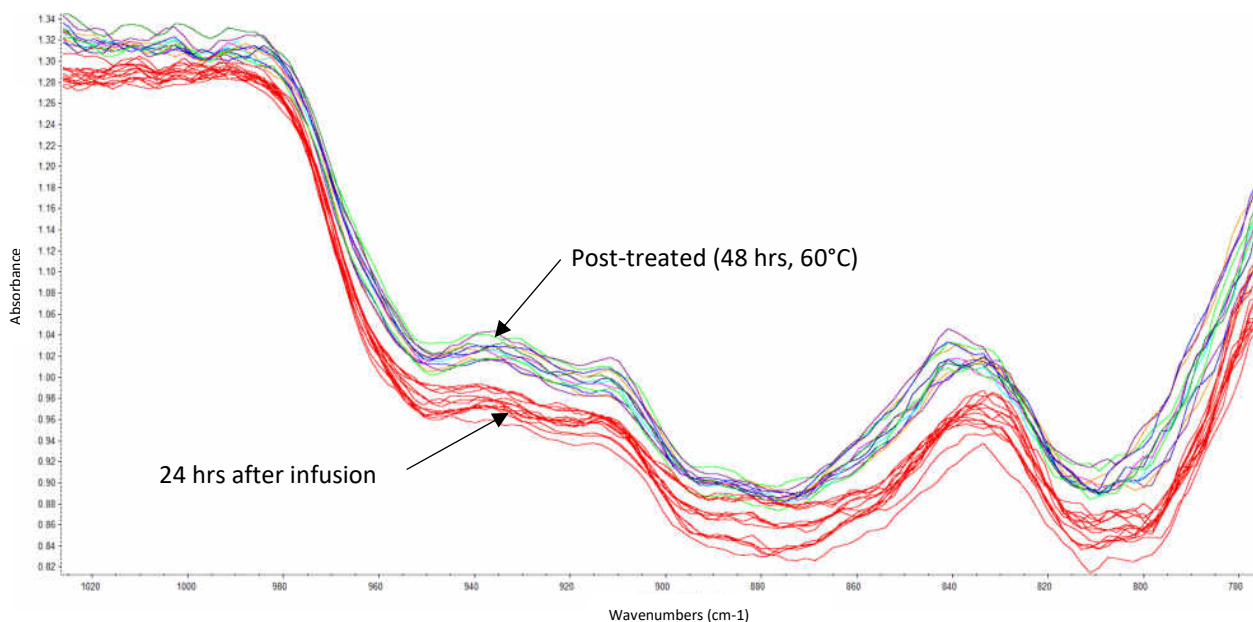
Figure 25: 24 hrs after infusion vs. post-treated GT-125 DRIFTs spectra, common scale
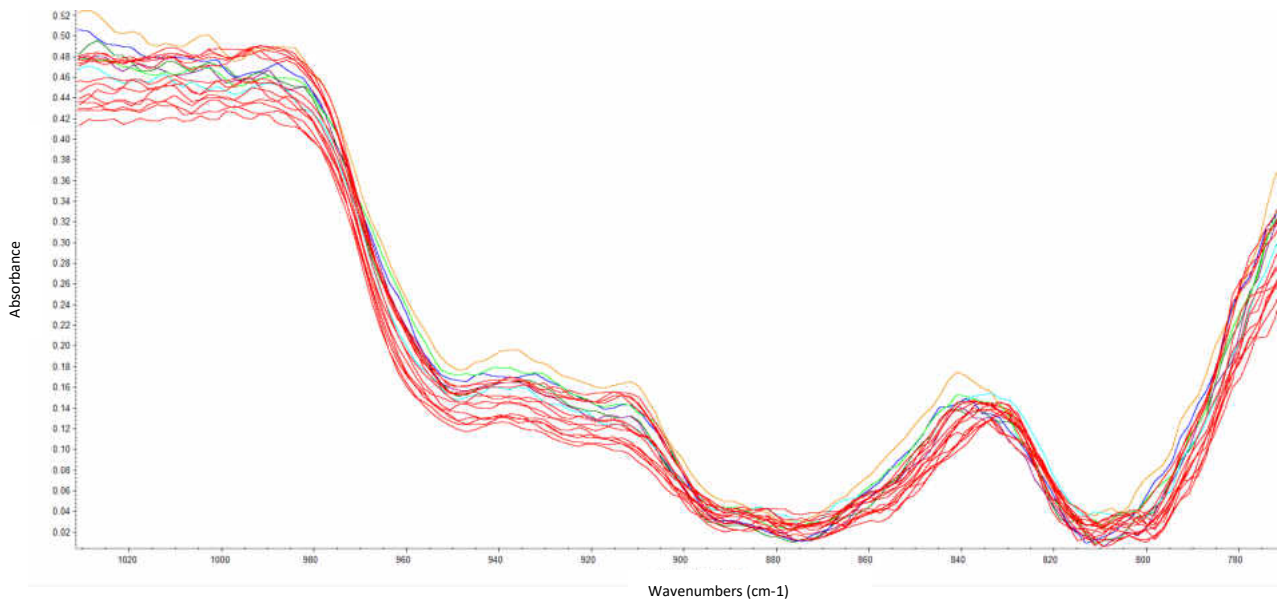
Figure 26: 24 hrs after infusion vs. post-treated GT-125 DRIFTs spectra, auto baseline correction

were corrected for scale variations using OMNIC's common scale function. This is necessary because the Agilent 4100 ExoScan scales the absorbance values based on the largest intensity peak collected during that scan. The common scale function relates all the spectra selected to a common absorbance scale based on the spectra with the largest absorbance value. This process assumes that the select spectra were taken of similar sample materials under similar operating conditions with the same sample interface attachment. Note the two distinct groupings of spectra which correspond to the two post-cure environments. This distinction is lost however with further processing and auto baseline correction is applied as seen in Figure 26.

While the spectra of the two extreme cure states seem to group together, it is evident as shown in Figure 25 that variation in these spectra can be observed. Similar to ATR, the effect of the reference sample was evaluated. Figure 27 shows that negligible variation is present between spectra if a single reference scan is taken at the beginning of the session and referenced throughout. Variation is present when the 4100 ExoScan is asked to take a new reference scan with each new sample scan as seen in Figure 28. While the observations are similar to those
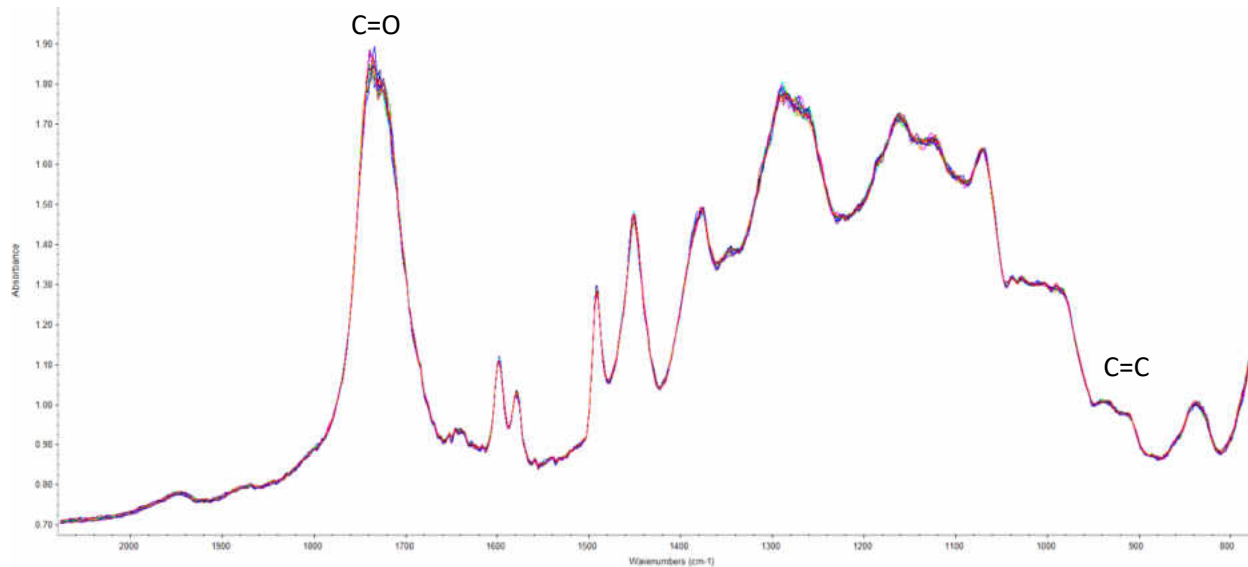
Figure 27: Overlay of DRIFTs spectra evaluated for repeatability, single reference sample
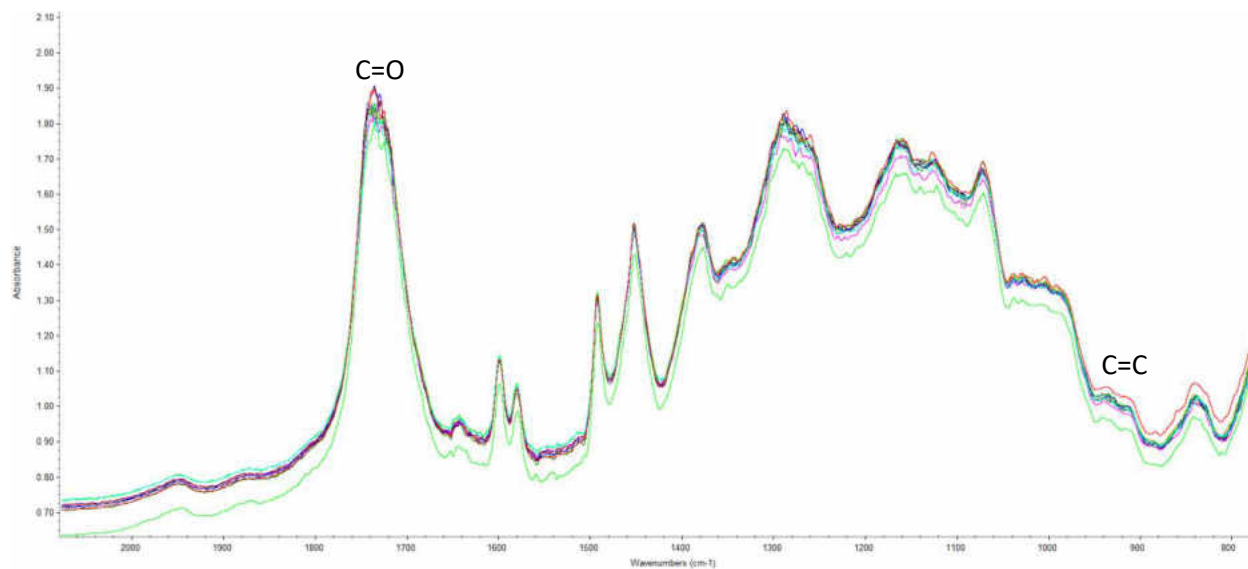
Figure 28: Overlay of DRIFTs spectra evaluated for repeatability, updated reference sample

found when analyzing the effect of the frequency of background scans on ATR spectra, the conclusion is much different. MicroLab PC, the software used in conjunction with the Agilent 4100 ExoScan defaults to the single reference scan case. Therefore, all previously presented DRIFTs data was collected under this condition. This means that the variation due to an updated reference scan is not present and more work needs to be completed to rectify the source of the observed variation.

In an attempt to further explore the resolution of the DRIFTs method as implemented with the Agilent 4100 ExoScan, a second series of samples were cast using the method outlined in Chapter 3.4.2. Spectra were taken from two sets of samples. First a series of samples were placed in the convection oven at 60°C for the following durations: 6, 24, 36, 48 hours. In addition, a second batch of samples were monitored at room temperature with spectra taken: 24, 36 and 48 hours after being removed from the mold. A summary of results can be seen in Appendix D. We see that while, in some instances, the distinction can be made between samples at different cure states, and results do not appear to follow a clear pattern or time progression. Furthermore, the results do not follow the established convention that the spectrum of a fully cured sample will display a weaker C=C signal at 912 cm^{-1} than that of a sample taken right out of the mold. This may be a result of several phenomena which are not well understood, however we are able to rule out the effect of the reference scan based on the work presented earlier.

The results presented above show that a distinction between the freshly demolded and post-treated samples does exist using DRIFTs, however, similar to ATR significant variation in the data is observed. Further work must be done to determine the sensitivity of this method to various cure states, beyond the two extreme cases, and to rectify and compensate for the source of variation in the data.

CHAPTER FIVE: CONCLUSIONS AND RECCOMENDATIONS

The purpose of this study was to evaluate the utility of the Agilent 4100 ExoScan for the purpose of determining the degree of cure (DOC) in an industrial composite. The materials used for sample fabrication were supplied by LM Wind Power, a global wind turbine blade manufacturer, and included: Polylite 413-575 unsaturated polyester resin, also known as GT-125, and an HM-glass fiber mat. Samples were fabricated using a process known as vacuum assisted resin transfer molding (VARTM) and cut to size using a diamond-tipped saw. Supplemental samples were also fabricated by pouring activated GT-125 resin into 3.8cm diameter ring forms.

This work has direct industrial application. Manufacturers utilizing laminar fiber composite materials are interested in monitoring DOC as a process control benchmark. Traditionally this has been done with destructive testing using methods such as differential scanning calorimetry, or by way of mechanical testing. Although effective, these processes are labor-intensive and time-consuming; it is for these reasons a non-destructive testing technique is desirable.

Samples were analyzed using two FTIR sampling technologies: attenuated total reflectance (ATR) and diffuse reflectance (DRIFTs). Both sampling interfaces are attachments designed to work seamlessly with the Agilent 4100 ExoScan and its companion software, MiroLab PC. Because the chemical composition is proprietary, a cure model proposed by de la Caba *et al.* [3] was used which leverages information relating to the styrene content to predict the

cure state of the bulk polyester matrix. In order to validate this cure model the GT-125 was analyzed using a Thermo Scientific Nicolet iS5 infrared spectrometer and outfitted with an iD1 transmission attachment. Spectra were taken from the resin at regular intervals until cure stabilized. Using OMNIC software to determine peak area, the time history was calculated using the proposed model. The model was validated using two criteria provided by LM Wind Power: 1) gelation occurred at approximately 2 hours and 2) cure stabilized approximately 24 hours after the initiator was introduced. The cure history confirmed both criteria.

Cure kinetics are time and temperature sensitive so in order to employ a system useful to industrial application, the FTIR method must be able to monitor cure as the reaction progresses in real time on an appropriate time scale.

The data presented in this study shows that neither ATR FTIR nor DRIFTs has the capability of monitoring the cure reaction on an acceptable time scale. At a 95% confidence interval, ATR FTIR has the capability of reliably determining the difference between only two cure states: freshly demolded (approx. 24 hours after resin infusion begins) and post-processed (an additional 14 hours at elevated temperature, 60°C). In some instances, ATR FTIR shows statistical significance on a smaller time scale however this pattern is not universal and differs tremendously sample to sample. It is possible to broaden the confidence interval however this would prove insufficient for industrial application. It is important that the method produces a confident estimate of the current cure state. Other possible indicators were also explored. Five combinations of sample and reference peaks were chosen in attempt to find one which shows statistical significance on the time scale of interest. No clear trends were found in this supplementary data set.

An exploratory investigation of DRIFTs was performed using GT-125 resin samples. The data gathered via DRIFTs led to similar conclusions; only samples subjected to vastly different post-processing conditions can be differentiated via DRIFTs.

In order to provide a clearer picture of cure using FTIR spectra, further study needs to be done to rectify the cause of variation in ATR FTIR data and identify the source of the infrared bands present in the GT-125 spectrum. If sources of error in each step of the data processing sequence can be identified and quantified this information could be used to introduce a series of correction factors which may help uncover underlying trends. In order to do this, however, it is crucial to gain understanding of the algorithms Agilent implements to transform the raw inferogram into an infrared spectrum. Additionally, further quantification of DRIFTs must be completed in order to effectively evaluate the two methods side-by-side. This can be accomplished by first performing a DOE to choose optimum sampling parameters to reduce the effect of noise. Additionally, work must be done to verify the C=C peak at 912 cm^{-1} has not shifted as a result of the sampling method or sample preparation.

To further explore the utility of FTIR in cure kinetic applications, a larger sample set should be used and more spectra need to be gathered. The state of cure is time dependent so in order to successfully expand the scope of data collection, a method of time compensation must be investigated. Additional recommendations include: correlating each spectra with a coordinate system to track the changes in the spectra over the surface of the sample and preparing samples with uniform surface finish, removing possibility of spectral defects on surface impurities like scratches.

frequency, cm^{-1}	bond	functional group
3640–3610 (s, sh)	O–H stretch, free hydroxyl	alcohols, phenols
3500–3200 (s,b)	O–H stretch, H–bonded	alcohols, phenols
3400–3250 (m)	N–H stretch	1°, 2° amines, amides
3300–2500 (m)	O–H stretch	carboxylic acids
3330–3270 (n, s)	–C≡C–H: C–H stretch	alkynes (terminal)
3100–3000 (s)	C–H stretch	aromatics
3100–3000 (m)	=C–H stretch	alkenes
3000–2850 (m)	C–H stretch	alkanes
2830–2695 (m)	H–C=O: C–H stretch	aldehydes
2260–2210 (v)	C≡N stretch	nitriles
2260–2100 (w)	–C≡C– stretch	alkynes
1760–1665 (s)	C=O stretch	carbonyls (general)
1760–1690 (s)	C=O stretch	carboxylic acids
1750–1735 (s)	C=O stretch	esters, saturated aliphatic
1740–1720 (s)	C=O stretch	aldehydes, saturated aliphatic
1730–1715 (s)	C=O stretch	α, β–unsaturated esters
1715 (s)	C=O stretch	ketones, saturated aliphatic
1710–1665 (s)	C=O stretch	α, β–unsaturated aldehydes, ketones
1680–1640 (m)	–C=C– stretch	alkenes
1650–1580 (m)	N–H bend	1° amines
1600–1585 (m)	C–C stretch (in–ring)	aromatics
1550–1475 (s)	N–O asymmetric stretch	nitro compounds
1500–1400 (m)	C–C stretch (in–ring)	aromatics
1470–1450 (m)	C–H bend	alkanes
1370–1350 (m)	C–H rock	alkanes
1360–1290 (m)	N–O symmetric stretch	nitro compounds
1335–1250 (s)	C–N stretch	aromatic amines
1320–1000 (s)	C–O stretch	alcohols, carboxylic acids, esters, ethers
1300–1150 (m)	C–H wag (–CH$_2$X)	alkyl halides
1250–1020 (m)	C–N stretch	aliphatic amines
1000–650 (s)	=C–H bend	alkenes
950–910 (m)	O–H bend	carboxylic acids
910–665 (s, b)	N–H wag	1°, 2° amines
900–675 (s)	C–H "oop"	aromatics
850–550 (m)	C–Cl stretch	alkyl halides
725–720 (m)	C–H rock	alkanes
700–610 (b, s)	–C≡C–H: C–H bend	alkynes
690–515 (m)	C–Br stretch	alkyl halides

m–medium, w–weak, s–strong, n–narrow, b–broad, sh–sharp

StdOrder	RunOrder	CenterPt	Blocks	No of Scans	Resolution	Appodization	Smoothing	No of Runs	Mean RMS	SNR
22	1	1	2	-1	-1	-1	-1	5	0.000946	3.350446
29	2	1	2	1	1	1	-1	5	0.000306	8.83659
32	3	1	2	-1	1	-1	1	5	0.000314	9.959292
41	4	0	2	0	0	0	0	5	0.000424	6.057078
25	5	1	2	1	1	-1	-1	5	0.000384	6.824224
35	6	1	2	1	-1	1	1	5	0.00034	6.155664
38	7	0	2	0	0	0	0	5	0.000352	4.58706
37	8	1	2	1	1	1	1	5	0.000276	9.234358
31	9	1	2	1	-1	-1	1	5	0.00034	6.989796
40	10	0	2	0	0	0	0	5	0.00038	5.123252
27	11	1	2	1	-1	1	-1	5	0.000364	5.63951
33	12	1	2	1	1	-1	1	5	0.000252	9.307148
24	13	1	2	-1	1	-1	-1	5	0.000508	7.543028
30	14	1	2	-1	-1	-1	1	5	0.000538	6.59894
36	15	1	2	-1	1	1	1	5	0.00033	7.926296
42	16	0	2	0	0	0	0	5	0.00035	5.319044
26	17	1	2	-1	-1	1	-1	5	0.000604	5.768286
34	18	1	2	-1	-1	1	1	5	0.000504	6.298432
23	19	1	2	1	-1	-1	-1	5	0.000466	5.696744
28	20	1	2	-1	1	1	-1	5	0.000408	8.366174
39	21	0	2	0	0	0	0	5	0.000348	7.249554
15	22	1	1	-1	1	1	1	5	0.00033	5.294354
18	23	0	1	0	0	0	0	5	0.000336	5.187188
10	24	1	1	1	-1	-1	1	5	0.00039	3.28189
12	25	1	1	1	1	-1	1	5	0.00029	5.190034
14	26	1	1	1	-1	1	1	5	0.000352	3.483246
9	27	1	1	-1	-1	-1	1	5	0.000584	2.828918
7	28	1	1	-1	1	1	-1	5	0.000504	2.833928
1	29	1	1	-1	-1	-1	-1	5	0.001036	1.141584
13	30	1	1	-1	-1	1	1	5	0.000524	2.81702
6	31	1	1	1	-1	1	-1	5	0.00047	2.251858
19	32	0	1	0	0	0	0	5	0.000348	4.883916
16	33	1	1	1	1	1	1	5	0.00027	5.80605
11	34	1	1	-1	1	-1	1	5	0.000366	4.669432
8	35	1	1	1	1	1	-1	5	0.00035	3.8894675
3	36	1	1	-1	1	-1	-1	5	0.000664	2.842456
17	37	0	1	0	0	0	0	5	0.00036	4.816268
4	38	1	1	1	1	-1	-1	5	0.000474	2.839892
21	39	0	1	0	0	0	0	5	0.00033	6.021778
5	40	1	1	-1	-1	1	-1	5	0.000708	1.843498
2	41	1	1	1	-1	-1	-1	5	0.000626	1.753672
20	42	0	1	0	0	0	0	5	0.000318	5.355902

3A-3
At(697.7)/At(Ref)

3A-4
At(697.7)/At(Ref)

3A-5
At(697.7)/At(Ref)

3A-6
At(697.7)/At(Ref)

3A-7
At(697.7)/At(Ref)

3A-8
At(697.7)/At(Ref)

3A-9
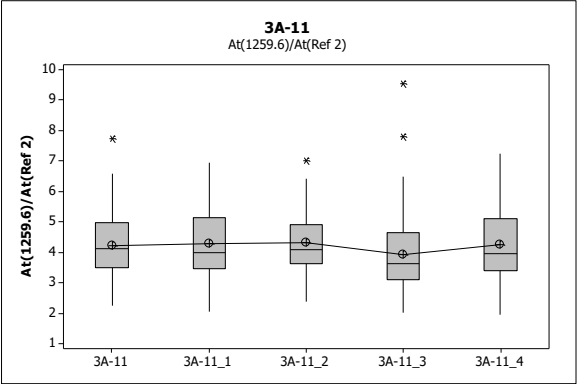At(697.7)/At(Ref)

3A-10
At(697.7)/At(Ref)
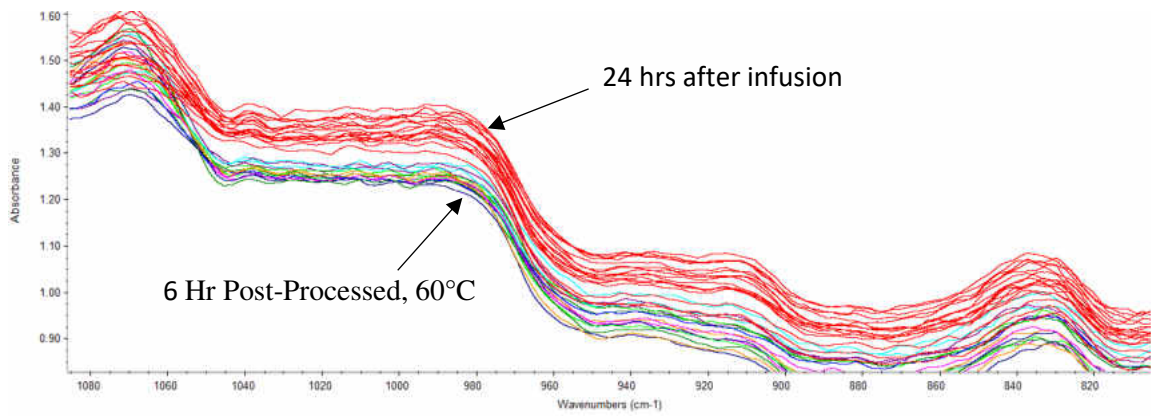
64

3A-11
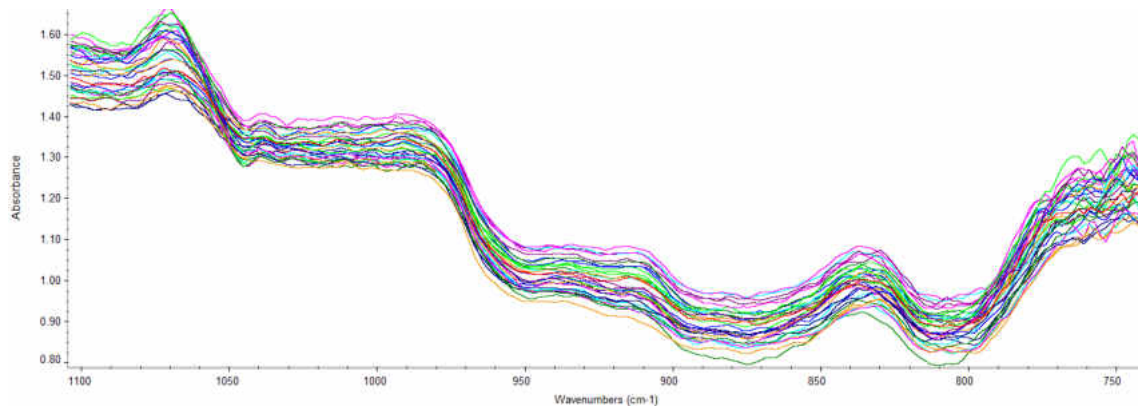At(1259.6)/At(Ref 2)
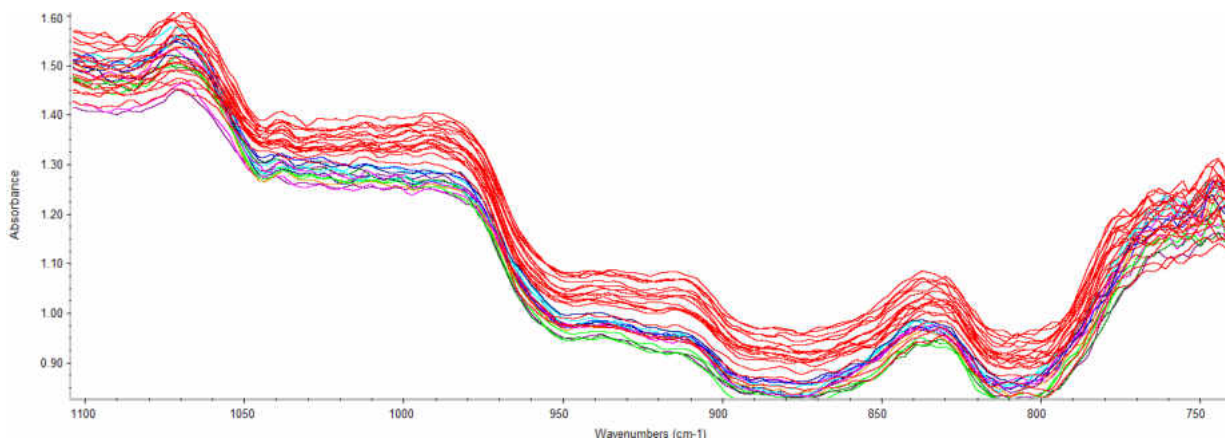

3A-12
At(1259.6)/At(Ref 2)
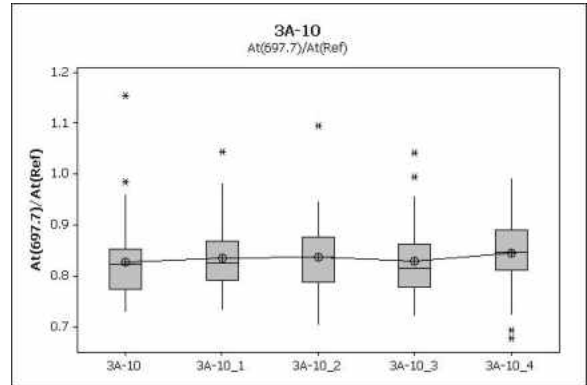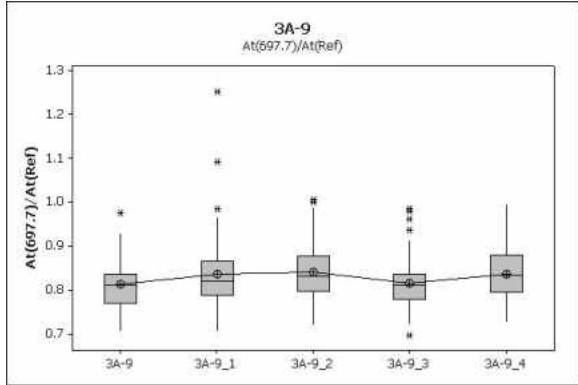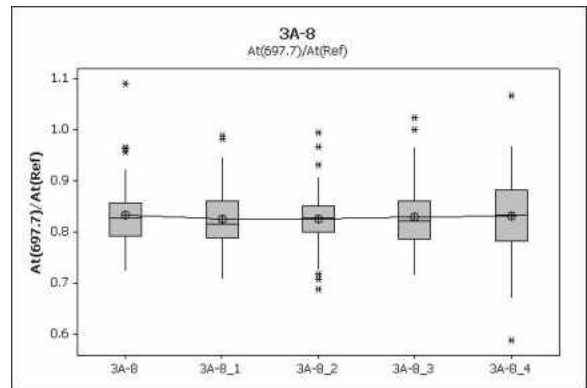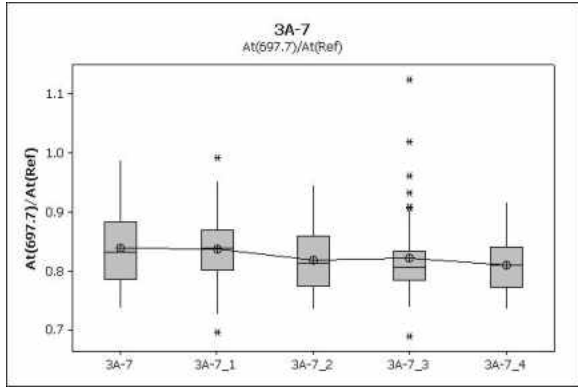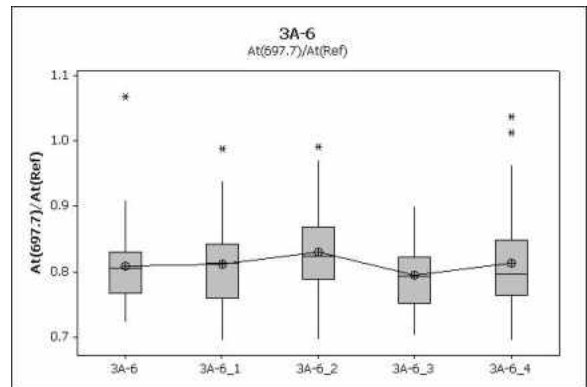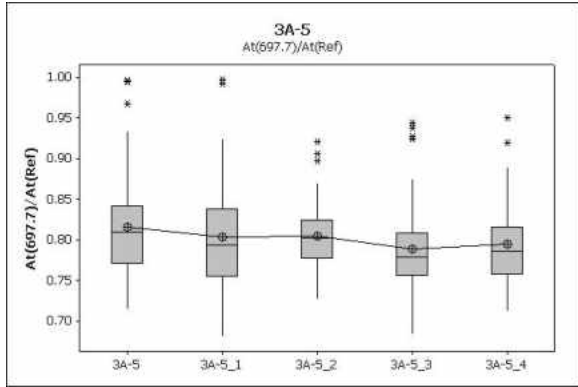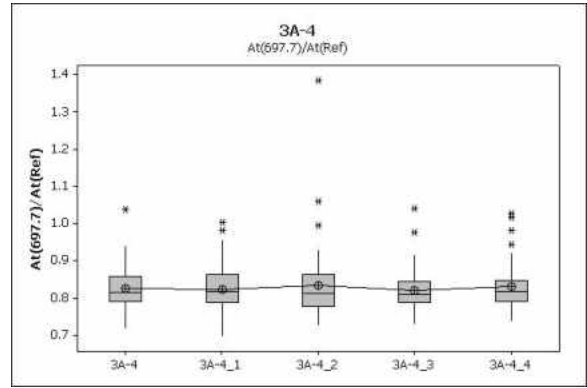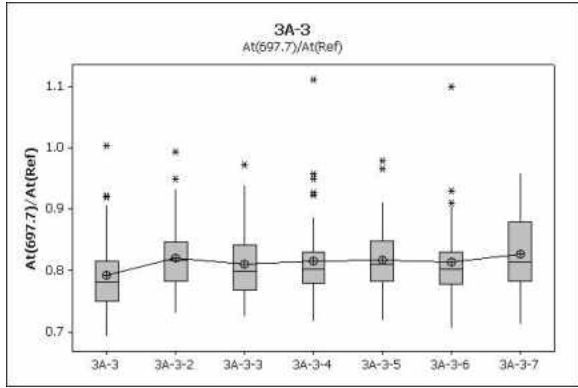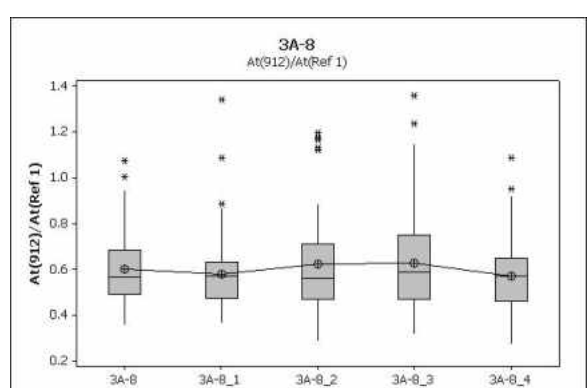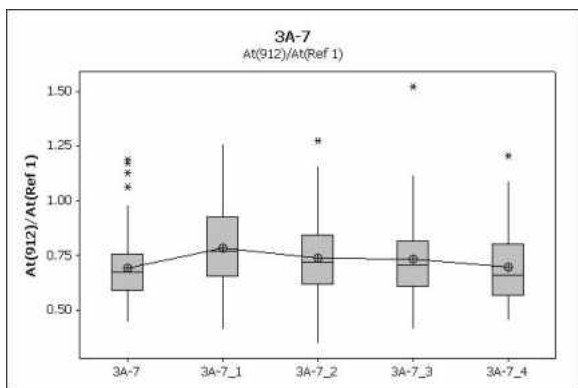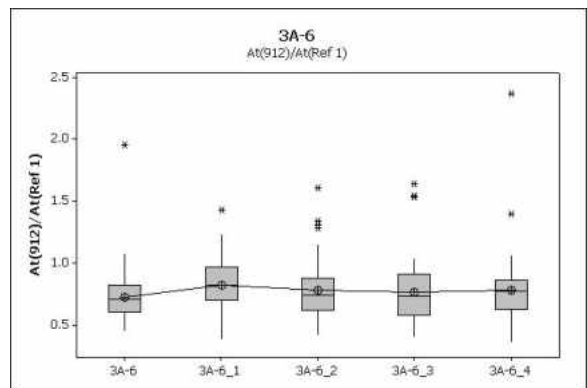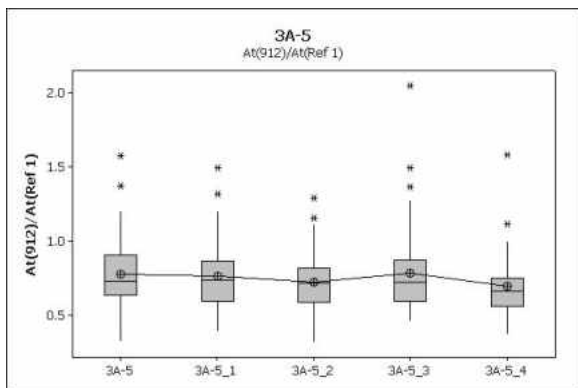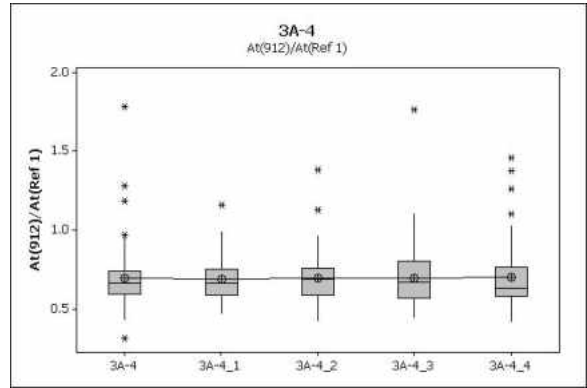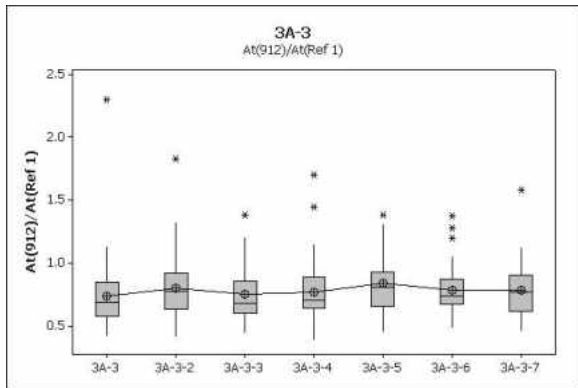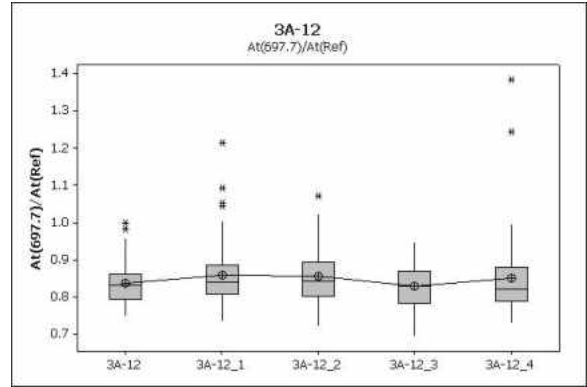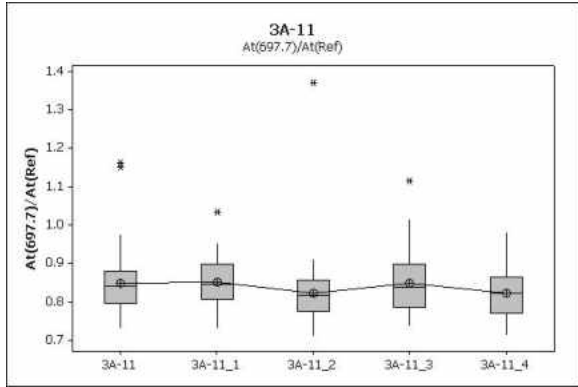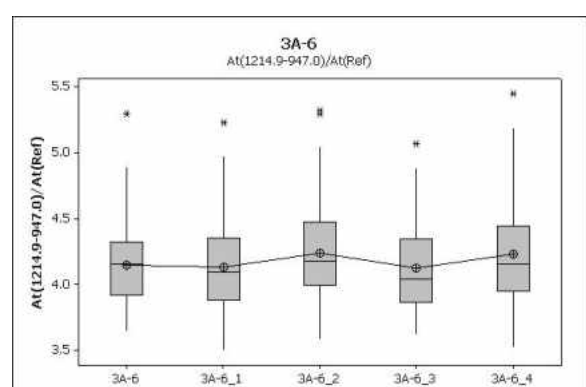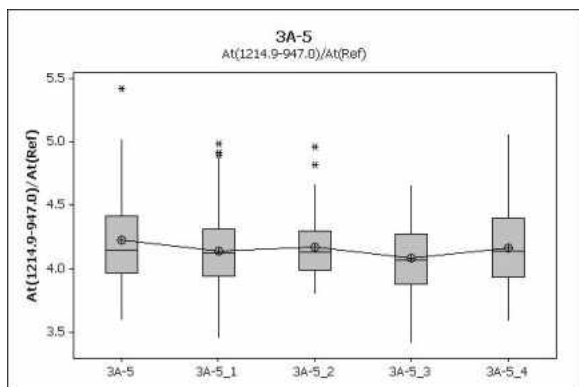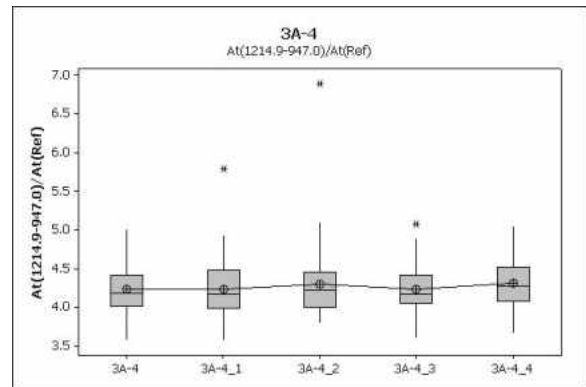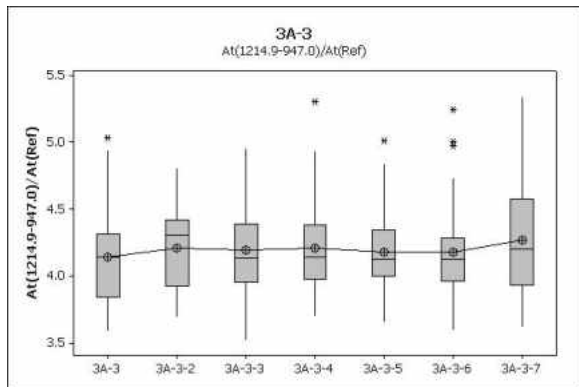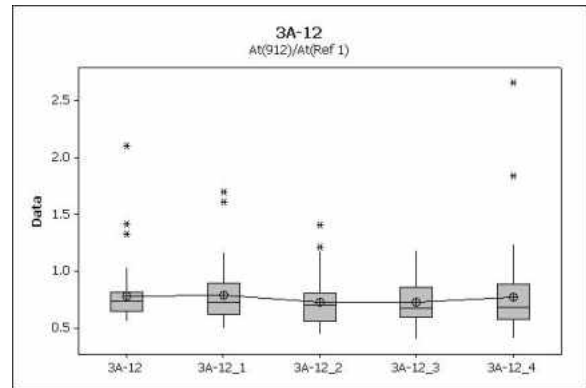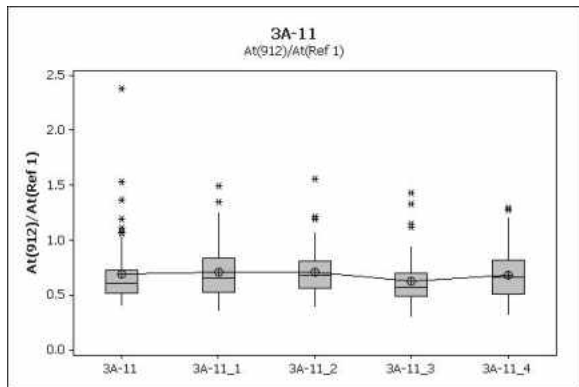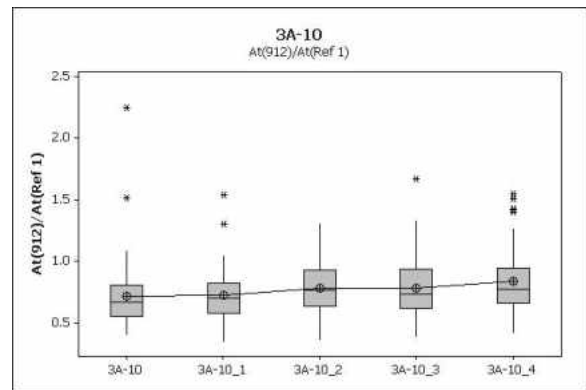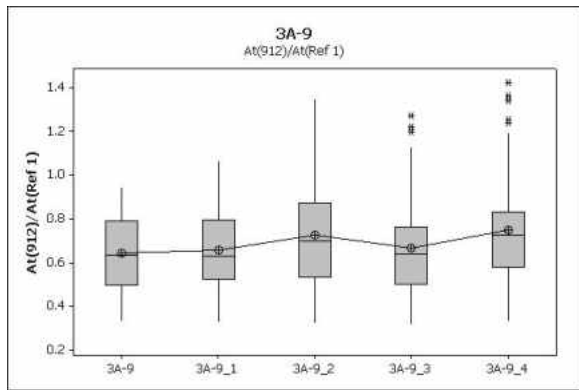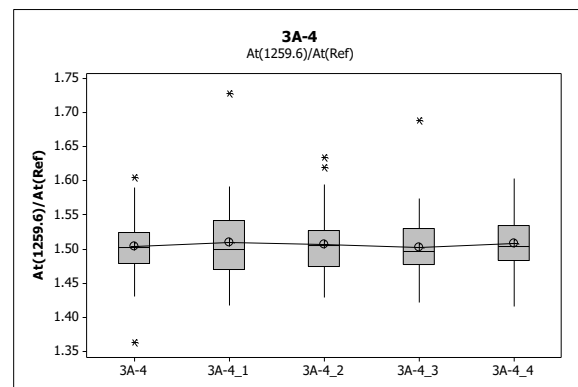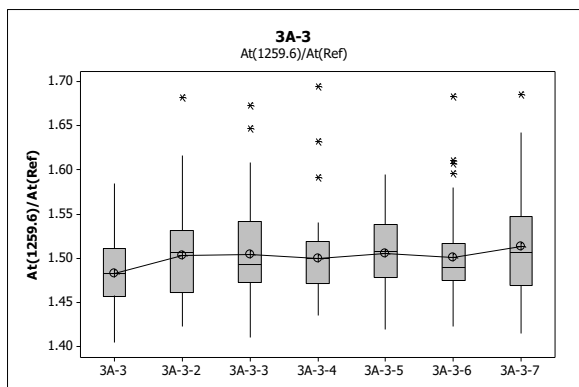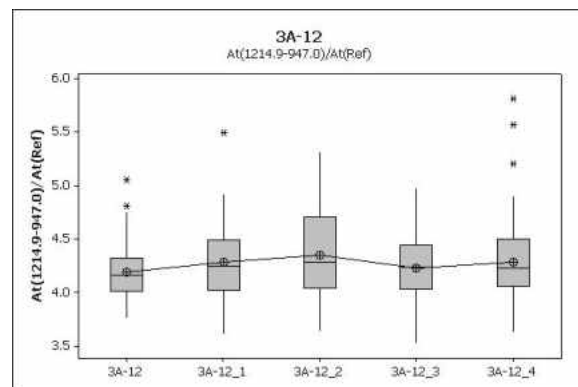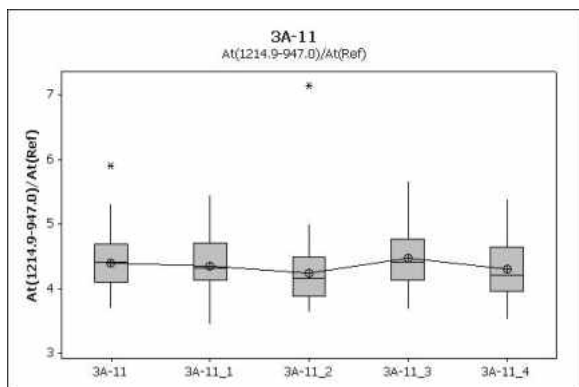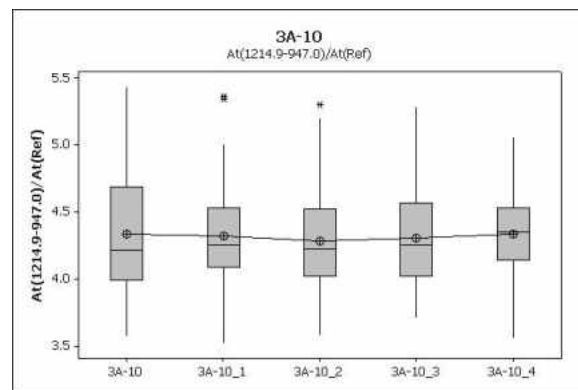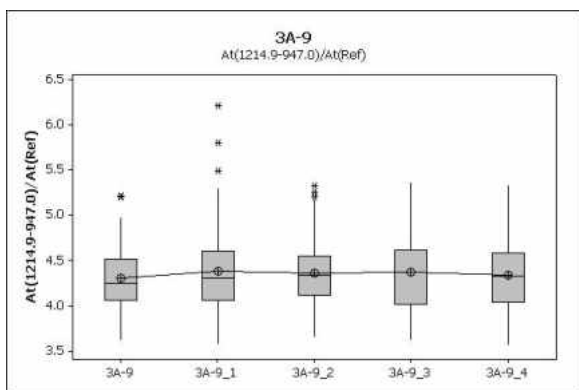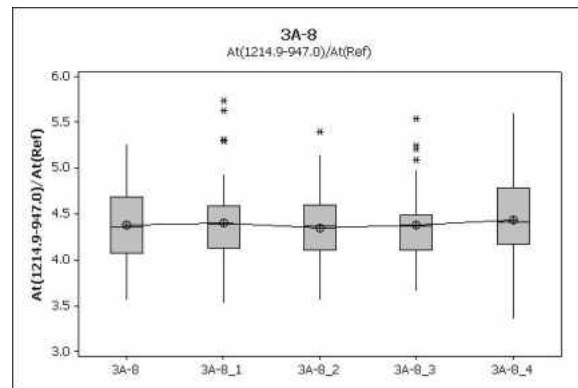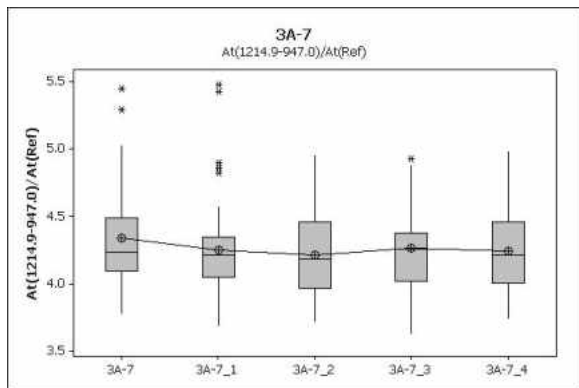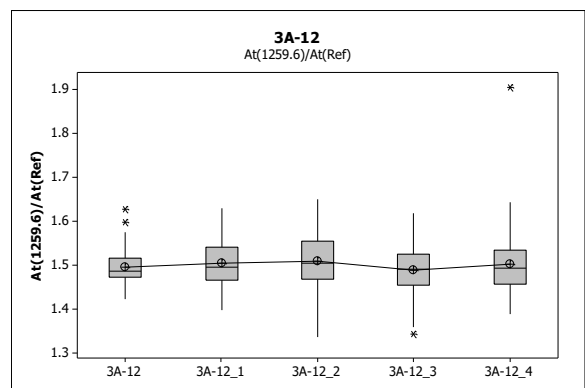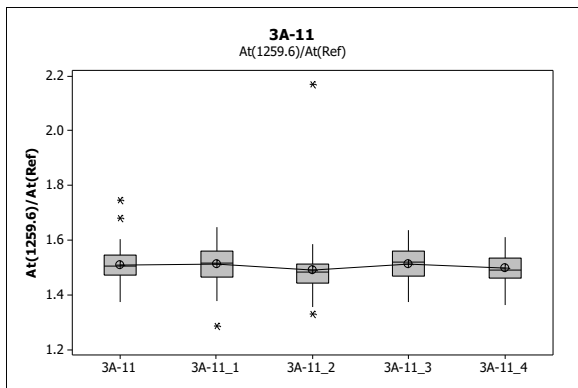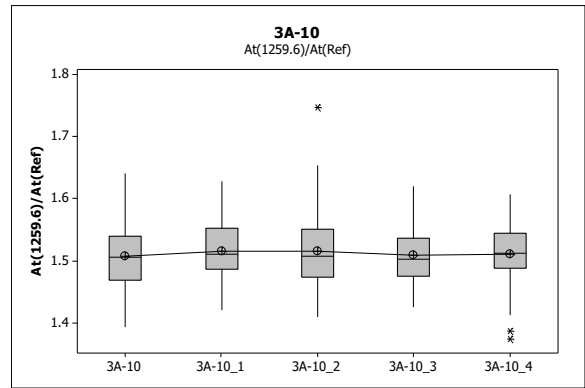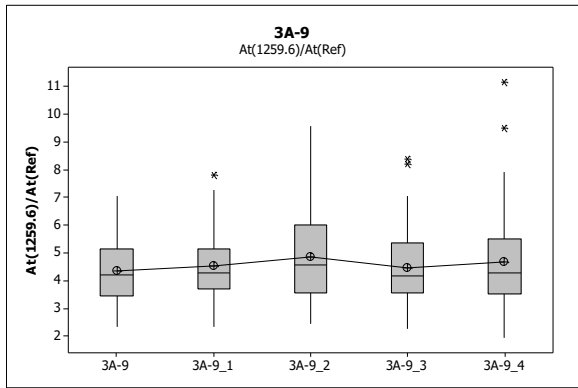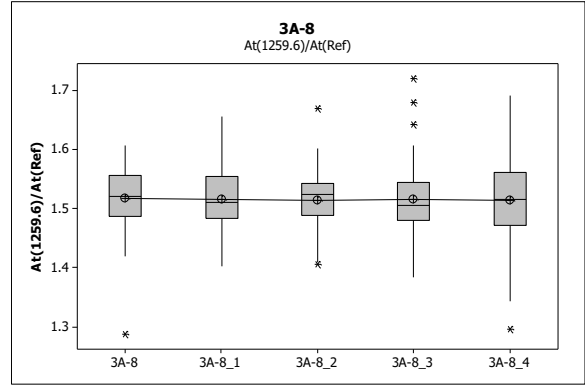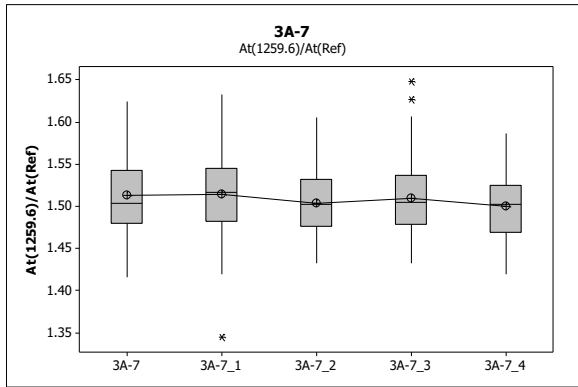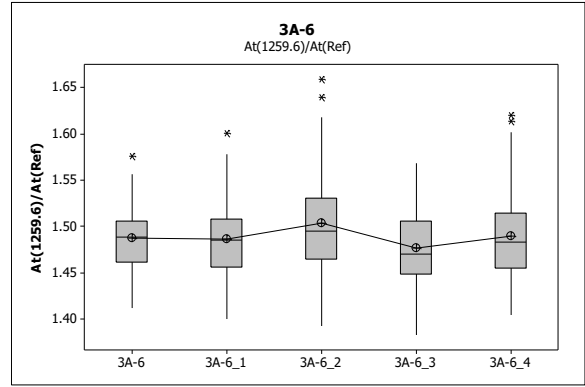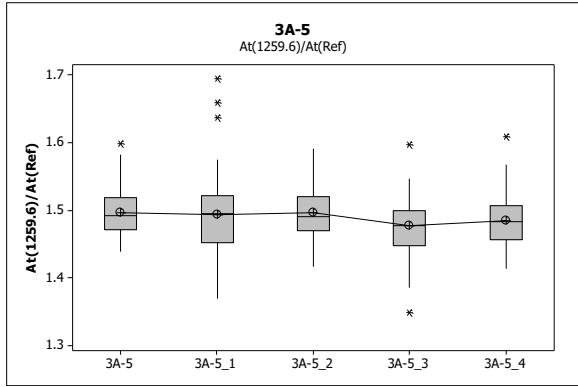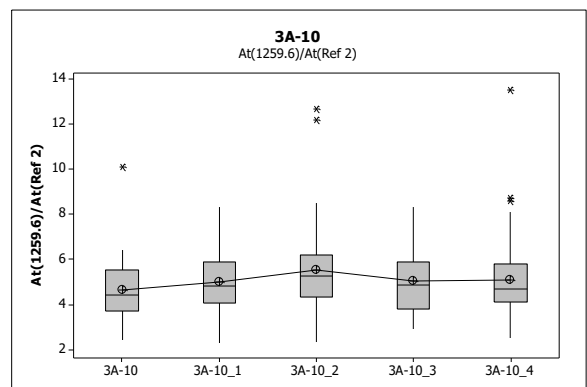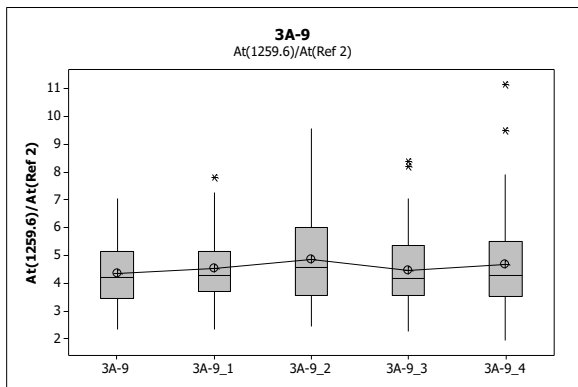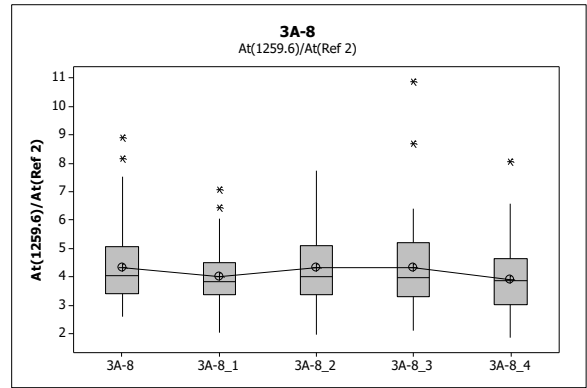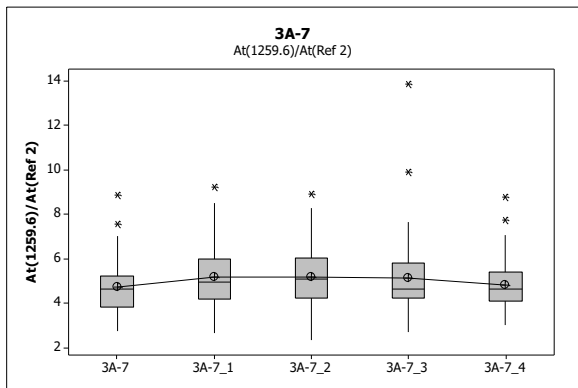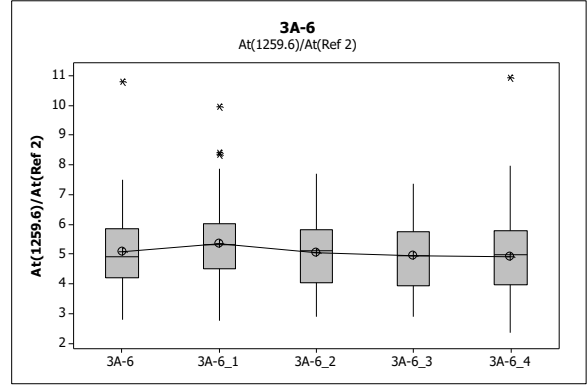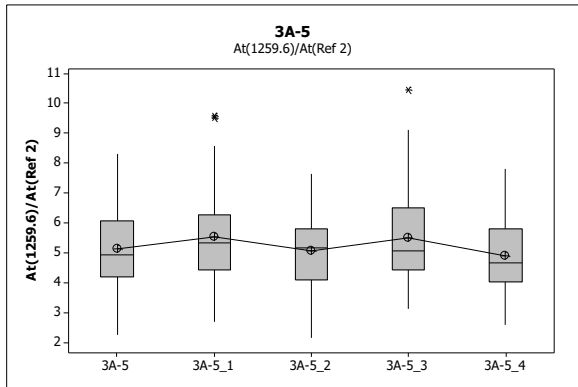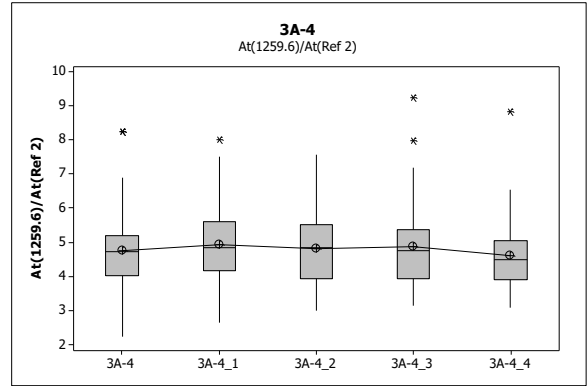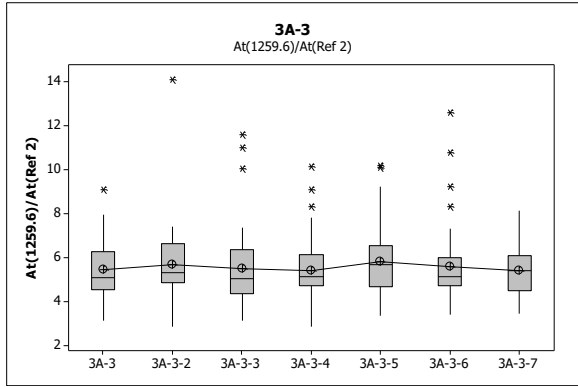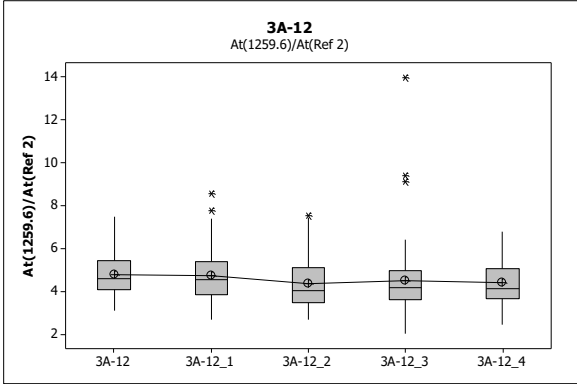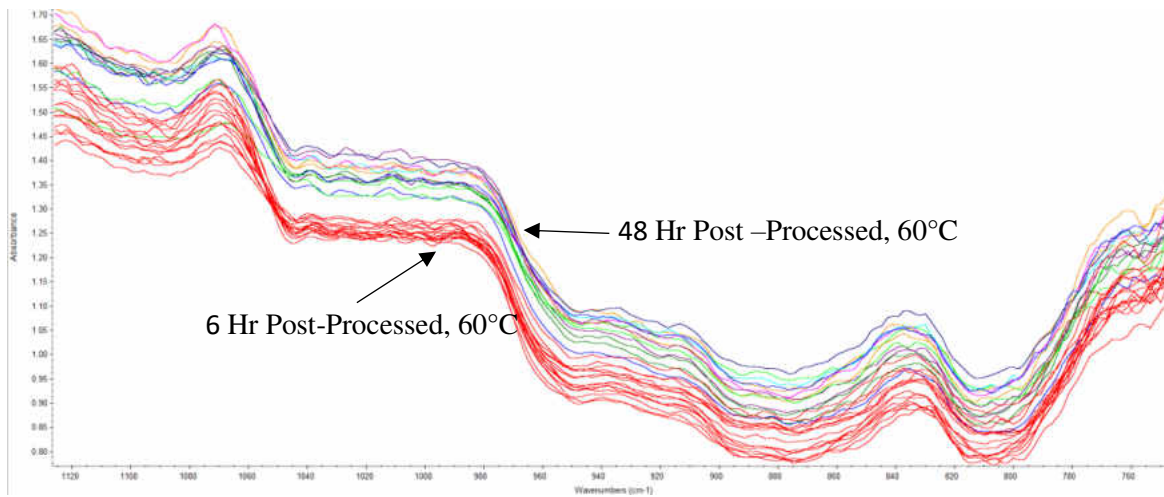
Appendix D
Additional DRIFTs Results

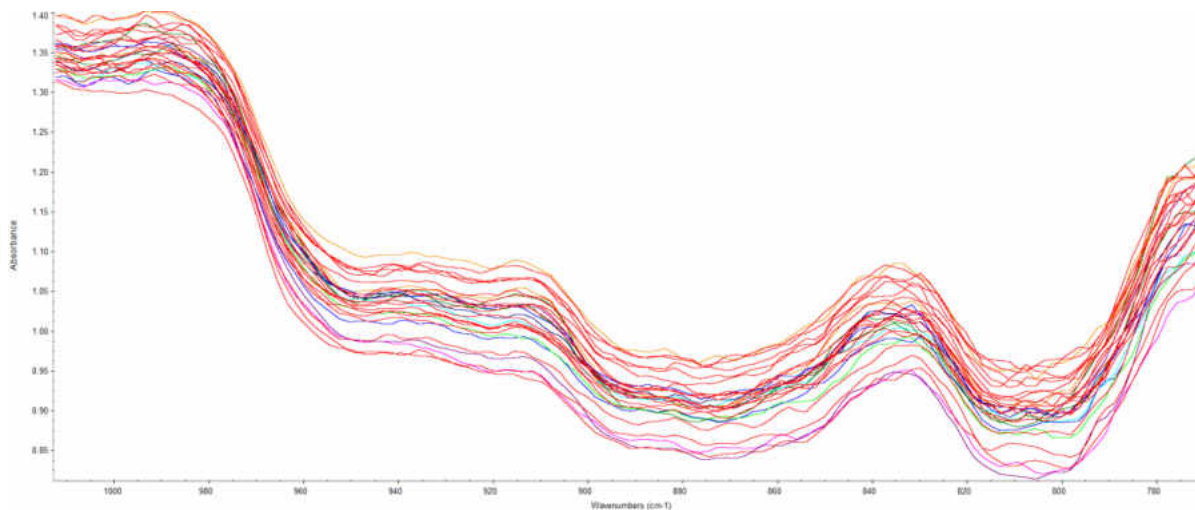*Overlay of DRIFTs spectra: 24 hrs after resin infusion vs 6 hours at 60 ^{o}C*

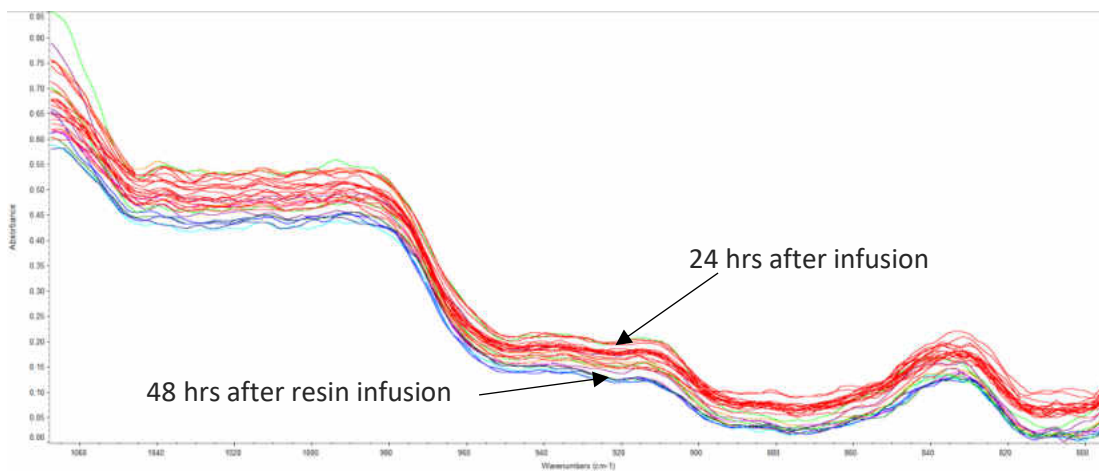*Overlay of DRIFTs spectra: 24 hrs after resin infusion vs 24 hours at 60 ^{o}C*

Overlay of DRIFTs spectra: 24 hrs after resin infusion vs 36 hours at 60 ^{o}C

Overlay of DRIFTs spectra: 6 hours at 60 ⁰C vs 48 hours at 60 ⁰C

Overlay of DRIFTs spectra: 24 hrs after resin infusion vs 48 hours after resin infusion

Overlay of DRIFTs spectra: 24 hrs after resin infusion vs 48 hrs after resin infusion, auto-baseline correct

REFERENCES

[1] Schwartz, M., 1992, *Composite Materials Handbook 2nd Edition,* McGraw-Hill, New York, NY.

[2] Peng, W., Riedl, B., 1995, "Thermosetting Resins," Journal of Chemical Education, **72**(7), pp. 587-592.

[3] de la Caba, K., Guerrero, P., et al., 1998, "Comparative Study by DSC and FTIR Techniques of an Unsaturated Polyester Resin Cured at Different Temperatures," Polymer International, **45**(5), pp. 333-338.

[4] George, B., McIntyre, P., Stuart, B., 1998, *Modern Infrared Spectroscopy,* John Wiley & Sons, Chichester, UK.

[5] Smith, B., 1996, *Fundamentals of Fourier Transform Infrared Spectroscopy,* CRC Press, Boca Raton, LA.

[6] Griffiths, P.R., de Haseth, J.A., 2007, *Fourier Transform Infrared Spectrometry,* John Wiley & Sons, Hoboken, NJ.

[7] Rein, A., 2014, "Advanced Fourier Transform Infrared Spectroscopy for Analyzing Damage in Aircraft Composites," DOT/FAA/TC-14/26, Federal Aviation Administration Aviation Research Division, Atlantic City, NJ.

[8] Agilent Technologies, 2016, "FTIR compact and Portable Systems," from https://www.agilent.com/en-us/products/ftir/ftir-compact-portable-systems/4100-ExoScan-series-ftir-(handheld).

[9] Thermo Fischer Scientific Inc., 2016, "TruDefender FTX/FTXi Handheld FTIR for Chemical Identification," from http://www.thermoscientific.com/en/product/trudefender-ftx-ftxi-handheld-ftir-chemical-identification.html.

[10] Turi, E. A., 1981, *Thermal Characterization of Polymeric Materials,* Academic Press Inc., Orlando, Fl.

[11] Pandita, S. D., Wang, L., Mahendran, R.S., et al., 2012, "Simultaneous DSC-FTIR Spectroscopy: Comparison of Cross-Linking Kinetics of an Epoxy/Amine Resin System," Thermochimica Acta, pp. 9-17.

[12] Scott, T. F., Cook, W. D., Forsythe, J. S., et al., 2003, "FTIR and ESR Spectroscopic Studies of Photopolymerization of Vinyl Ester Resins," Macromolecules, **36**(16), pp. 6066-6074.

[13] Lionetto, F., Maffezzoli, A., 2013, "Monitoring the Cure State of Thermosetting Resins by Ultrasound," Materials, **6**, pp. 3784-3804.

[14] Wang, L., Tomlin, A., Pandita, S.D., et al., 2016, "In-Situ Monitoring of Cross-Linking Reactions Using E-glass Fibres and Evanescent Wave Spectroscopy," Sensors and Actuators B, **236**, pp. 358-366.

[15] Aktak, A., Boyd, S.W., Shenoi, R.A., 2015, "Cure and Strain Monitoring of Novel Unsaturated Polyester/Phenolic Resin Blends in the Vacuum Infusion Process Using Fiber Bragg Gratings," Journal of Composite Materials, **49**(29), pp. 3599-3608.

[16] Teriault, R., Osswald, T.A., Stradins, L., 1997, "Properties of Thermosetting Polymers During Cure," Annual Technical Conference-Society of Plastics Engineers, **55**(1), pp. 766-773.

[17] Czash, P., Ilie, N., 2013, "In Vitro Comparison of Mechanical Properties and Degree of Cure of Bulk Fill Composites," Clinical Oral Investigations, **2013**(17), pp. 227-235.

[18] Labronici, M., Ishida, H., 1999, "Effect of Degree of Cure and Fiber Content on the Mechanical Properties and Dynamic Mechanical Properties of Carbon Fiber Reinforced PMR-15 Polyimide Composites," Polymer Composites, **20**(4), pp. 515-523.

[19] Material Specification: Direct roving HM-glass, 2014, LM Wind Power.

[20] Odian, George, 1991, *Principles of Polymerization,* John Wiley & Sons, New York, NY.

[21] Control Instruction: VARTM of test laminates, 2015, LM Wind Power.

[22] Odian, G., 1991, *Principles of Polymerization 3rd Edition,* John Wiley & Sons Inc., New York, NY.

[23] Herres, W., Gronholz, J., "Understanding FT-IR Data Processing," from http://www.ccmr.conell.edu/wp-content/uploads/sites/2/2015/11/Understanding_FTIR

[24] "Table of Characteristic Absorptions," from http://www.orgchem.colorado.edu/spectroscopy/specttutor/irchart.pdf